

Enhancements of Positioning for IoT Devices

GUODA TIAN

HATEM ODEALLA

MASTER'S THESIS

DEPARTMENT OF ELECTRICAL AND INFORMATION TECHNOLOGY

FACULTY OF ENGINEERING | LTH | LUND UNIVERSITY



Enhancements of Positioning for IoT Devices

By

Guoda Tian
gu7550ti-s@student.lu.se
Hatem OdetAlla
ha2125od-s@student.lu.se



LUND
UNIVERSITY

Department of Electrical and Information Technology
LUND UNIVERSITY

Supervisor: Fredrik Tufvesson (EIT)
Sha Hu (EIT)
Basuki Priyanto (Sony Mobile Communications AB)
Examiner: Fredrik Rusek (EIT)

MAY 2018

The aim of this thesis work is to find novel method(s), which enhance the performance of the existing Observed Time Difference of Arrival (OTDOA) positioning technique for Internet of Thing (IoT) devices introduced in Third Generation Partnership Project (3GPP) standard release 14. In this thesis work, NarrowBand IoT (NB-IoT) positioning is considered as the baseline. The scope includes the investigation on positioning reference signal (PRS), including modifying/replacing the current sequence generation by mathematical derivations, and modifying PRS configuration (e.g. increasing the density, new time/frequency resource grid).

Moreover, different correlator designs at the receiver side (either operating in time or frequency domain) have been analyzed in terms of performance and complexity. In addition, we also investigate the impact of PRS transmission extension either in time domain by sending multiple subframes or in frequency domain by utilizing more spectrum resources (using more Physical Resource Blocks (PRBs)).

Our results show that the current NB-IoT PRS resource mapping is already well designed. The newly suggested sequences and resource time/frequency grids influence the correlation properties which in turn affect the positioning accuracies. Increasing the number of resources for PRS transmission in time/frequency results in positioning accuracy improvements. Different sequences for PRS can lead to performance improvements with the cost of implementation complexity, and design flexibility. In addition, optimizing the original gold sequence shows a consistent good performance gain.

The Internet of Things (IoT) is a technology that allows the connectivity of smart devices and items to the Internet. IoT is becoming an increasingly growing topic since it has been estimated that billions of devices will be connected to the internet by 2025. The strong growth in IoT market will trigger a revolutionary in many industries, such as healthcare, agriculture, automotive, safety and security [1]. Thus, our daily life will be significantly affected by the development of this technology in the future. However, IoT will allow endless connections to take place which will open a door of many challenges such as strict requirements of devices power consumption, cost and complexity. Due to its wide range of applications, a lot of new standards have emerged to support IoT integration. Narrowband IoT (NB-IoT) is one of the newest cellular technologies which connects many low-cost devices in severe coverage situations with a lower power consumption and a longer battery lifetime.

In 3rd Generation Partnership Project (3GPP) release 14, positioning feature has been introduced to NB-IoT which will allow the location of devices to be determined by using the transmitted positioning reference signal (PRS) at the base-station side. This positioning technique is known as Observed Time Difference of Arrival (OTDOA), because the device position can be obtained by measuring the time of arrival of multiple signals from multiple base-stations. Then device position can be estimated by measuring the difference between the time of arrivals. Nevertheless, it is a quite challenging task to implement OTDOA in NB-IoT devices, due to the constraint of low cost and the strict power consumption requirements. Furthermore, extreme coverage conditions are expected for NB-IoT devices that affect received signal levels which in turn influences the positioning accuracy.

In this thesis, an OTDOA positioning simulation platform has been built. Several approaches have been implemented at transmitter side with an objective of improving positioning accuracy. The methods include generating various types of sequences, changing the original sequence mapping, and proposing new designs of the time-frequency resource grid in the system. It is shown that the current standard is well designed and has a good positioning performance. A lot of ideas have been implemented within this thesis scope, which lead to adequate accuracy under certain circumstances with acceptable complexity. For future work, more investigation of new sequences can be conducted to be used instead of the current standard. In addition, advanced low power receiver algorithms can be considered.

ACKNOWLEDGMENTS

We would like to thank Sony Mobile Communications AB in Lund, Sweden for giving us the opportunity to write our thesis about this topic within its premises. Special thanks to Dr. Basuki Priyanto for his continuous supervision, feedback, comments and advice throughout the whole thesis. Without his support, the finding of this thesis would have been impossible. Moreover, we are grateful to Dr. Peter C. Karlsson, director of research and standardization, for this thesis opportunity as well. Furthermore, we would like to express our gratitude to Prof. Fredrik Tufvesson, Prof. Fredrik Rusek and Dr. Sha Hu for helping to develop ideas and methods for the obstacles faced during our work. Finally, we would like to thank our families for their support the whole time we spent in Sweden and for their encouragement throughout our work and studies.

Guoda Tian
Hatem OdetAlla

LIST OF ACRONYMS

3GPP	3rd Generation Partnership Project
ACF	Auto-correlation Function
A-GNSS	Assisted Global Navigation Satellite System
AOA	Angle of Arrival
AWGN	Additive White Gaussian Noise
BS	Base Station
CAZAC	Constant Amplitude Zero Autocorrelation
CDF	Cumulative Distribution Functions
CP	Cyclic Prefix
DFT	Discrete Fourier Transform
DL	Downlink
E-CID	Enhanced Cell ID
eNB	Evolved Node-B
EPA	Extended Pedestrian A
E-SMLC	Evolved Serving Mobile Location Center
ETU	Extended Typical Urban
FFT	Fast Fourier Transform
GMLC	Gateway Mobile Location Center
GNSS	Global Navigation Satellite System
GPS	Global Positioning System
GSM	Global System for Mobile communications
IFFT	Inverse Fast Fourier Transform
IoT	Internet of Things
LBS	Location Based Services
LPP	LTE Positioning Protocol
LPWAN	Low Power Wide Area Network
LTE	Long Term Evolution

LTE-M	Long Term Evolution, category M1
MCL	Maximum Coupling Loss
MF	Matched Filter
MME	Mobility Management Entity
MMSE	Minimum Mean Square Error
MTC	Machine Type Communication
NB-IoT	Narrowband-Internet of Things
NPRS	Narrowband Positioning Reference Signals
OFDM	Orthogonal Frequency Division Multiplexing
OTDOA	Observed Time Difference of Arrival
PAN	Personal Area Networks
PAPR	Peak to Average Power Ratio
PCI	Physical Cell Identity
PDN-GW	Packet Data Network Gateway
PN	Pseudo Noise
PRACH	Physical Random Access Channel
PRB	Physical Resource Block
PRS	Positioning Reference Signal
PSS	Primary Synchronization Signal
QPSK	Quadrature Phase Shift Keying
RB	Resource Block
RE	Resource Element
RSTD	Reference Signal Time Difference
RTT	Round-Trip Time
SLP	Service Location Protocol
S-GW	Serving Gateway
SINR	Signal to Interference and Noise Ratio
SNR	Signal to Noise Ratio
SSS	Secondary Synchronization Signal
TDOA	Time Difference of Arrival
TOA	Time of Arrival
UE	User Equipment
UL	Uplink
ZC	Zadoff-Chu
ZCC	Zero Cross Correlation
ZF	Zero Forcing

TABLE OF CONTENTS

	Page
List of Tables	xi
List of Figures	xiii
1 Introduction	1
2 Background	3
2.1 The Internet of Things	3
2.2 NB-IoT	4
2.3 NB-IoT Frame Structure	5
2.4 OFDM Transmission	5
3 OTDOA Positioning	7
3.1 Introduction	7
3.2 OTDOA positioning	8
3.3 Positioning Procedure	9
3.4 Narrowband Positioning Reference Signal (NPRS)	9
3.5 Reference Signal Time Difference (RSTD) measurement	11
3.6 Time of Arrival (TOA)	11
3.7 Time Difference of Arrival (TDOA)	12
4 Design of Reference Signal and Configuration	13
4.1 PRS Density	13
4.2 Different Time Frequency Resource Block Designs	16
4.2.1 Proposed Design Scheme 1	17
4.2.2 Proposed Design Scheme 2	18
4.2.3 Proposed Design Scheme 3	19
4.2.4 Proposed Design Scheme 4	20
4.3 Optimizing the Original Gold Sequence	20
4.4 Investigation on PRS Sequences	21
4.4.1 Zadoff-Chu Sequence	22

TABLE OF CONTENTS

4.4.2	Hadamard-Walsh Codes	25
4.4.3	Zero Cross-Correlation Complementary (ZCC) Sequences	26
4.4.4	Barker Sequence Matrix	26
4.5	Expansion of PRS transmission in Time and/or Frequency	28
5	Receiver Design	31
5.1	Channel models	31
5.1.1	Frequency Flat Fading Channel Model	31
5.1.2	Frequency Selective Fading Channel Model	33
5.2	Receiver Structure	34
5.3	Combiner Design	35
5.3.1	Incoherent combiner	35
5.3.2	Coherent combiner	35
5.4	Correlator design	37
5.4.1	Time domain correlator	37
5.4.2	Frequency domain correlator	38
5.4.3	Computation Complexity Analysis	39
5.5	Peak Detector	40
5.5.1	Introduction	40
5.5.2	Resolution Enhancement by Correlation Interpolation	41
5.5.3	The Position Estimation Solutions	41
6	Simulation Results	45
6.1	Simulation Assumptions	46
6.2	PRS density	47
6.3	Different Time Frequency Resource Grid Design	47
6.4	Different Sequence Comparison	49
6.5	Gold Sequence Optimization	52
6.6	Multiple Subframes processing	53
6.7	Multiple PRBs processing	55
6.8	EPA channel	56
6.9	Low SNR Analysis	59
7	Summary	61
	Bibliography	63

LIST OF TABLES

TABLE	Page
5.1 PDP of EPA Channel Model	33
5.2 PDP of ETU Channel Model	34
5.3 Computation Complexity Analysis	39
6.1 Simulation Parameters Settings	48
6.2 Sequence Comparison	53

LIST OF FIGURES

FIGURE	Page
2.1 NB-IoT Deployment Scenarios	4
2.2 LTE Resource Grid	5
2.3 OFDM Wireless System Structure	6
3.1 OTDOA Basic Principle [2]	8
3.2 LTE Location Service Architecture [2]	9
3.3 NPRS Mapping to Resource Elements	11
3.4 TOA Principle	12
4.1 Tx Process	14
4.2 Original Resource Grid	15
4.3 Three PRSs Resource Grid	15
4.4 Four PRSs Resource Grid	16
4.5 AutoCorrelation of 3PRS vs Original	16
4.6 AutoCorrelation of 4PRS vs Original	17
4.7 Resource Grid Design 1	17
4.8 Normalized ACF of 6 sub-carriers Spacing	18
4.9 Resource Grid Design 2	18
4.10 ACF of different sub-carriers Spacing	19
4.11 Resource Grid Design 3	19
4.12 Resource Grid Design 4	20
4.13 ZC Constellation Diagram	23
4.14 ZC sequence of length 839 Autocorrelation	23
4.15 Cross Correlation of ZC Sequence of length 63 and roots 25 29 and 34	24
4.16 ZCC Sequence Constellation Diagram	27
4.17 The Autocorrelation of Barker Sequence	27
4.18 Multiple Subframe Transmission Procedure	29
4.19 ACF of Gold sequence with different PRBs Configuration	29
5.1 Basic Large Scale Fading Channel	32

5.2	Frequency Flat Fading Channel	32
5.3	Receiver Structure	35
5.4	Frequency Correlator	39
5.5	eNB's Map [3]	42
5.6	UEs dropped under certain cell	42
5.7	Less dropped UE with better Estimator	43
6.1	GUI Screen	45
6.2	Sites Cell Grid	46
6.3	Failed Detected UEs	47
6.4	4 eNBs performance	48
6.5	6 eNBs performance	49
6.6	Different 2 PRS designs performance	49
6.7	Positioning Accuracy of Walsh-Hadamard Sequence	50
6.8	Comparisons of different ZC sequences with the Gold Sequence	50
6.9	Comparisons of ZCC with the Gold Sequence	50
6.10	Comparisons of Barker with the Gold Sequence	51
6.11	PAPR of various sequences in OFDM scheme	52
6.12	PAPR of various sequences in SC-FDMA scheme	52
6.13	Optimized Sequence vs original for cell IDs from 1 to 6 1st approach	53
6.14	Optimized Sequence vs original for cell IDs from 7 to 12	53
6.15	Optimized Sequence vs original for cell IDs from 13 to 18	54
6.16	Optimized Sequence vs original for cell IDs from 1 to 6 2nd approach	54
6.17	Coherent vs Incoherent Combining	54
6.18	Multiple Subframes cell IDs from 0 to 5	55
6.19	Multiple Subframes cell IDs from 1 to 6	55
6.20	Multiple PRBs vs single PRB	56
6.21	Multiple PRBs 10 subframes	56
6.22	Multiple PRBs 30 subframes	57
6.23	Multiple PRBs and subframes	57
6.24	Multiple Subframes vs Single Subframe EPA Ch. 10dB SNR and 3Hz doppler	58
6.25	Different PRBs configuration Performance	58
6.26	EPA channel Original and Optimized Positioning Accuracy	58
6.27	Low SNR with a single PRB	59
6.28	Low SNR EPA Channel	59
6.29	Low SNR with 4 PRBs	60
6.30	Low SNR with 2 PRBs	60
6.31	Low SNR ETU Channel with 3Hz doppler	60

INTRODUCTION

The cellular market has been under continuous development for the last decades and rapid research in many areas are still ongoing with all aims to improve the end user experience. One of these areas is Location Based Services (LBS) for Internet of Things (IoT) devices, which attracts a lot of attention in recent years. Future trends show the necessity to enhance the current existing positioning methods to achieve a quicker and more accurate estimation of a user's position due to the sheer number of services demanded. Thus, positioning plays a vital role in the IoT standard. As to positioning, there are several technologies which have already been developed a few decades ago and nowadays these positioning technologies are already matured, such as Global Navigation Satellite System (GNSS). GNSS positioning is the most famous method used in positioning but it is not suitable to be applied for IoT devices because of high cost and power consumption, besides poor coverage conditions of IoT devices [4]. Massive efforts have been spent from 3GPP to find other methods that can be used for position estimation. In the meantime, OTDOA catches a lot of attention and is applied for positioning in NB-IoT devices.

The purpose of this thesis is to investigate and enhance the OTDOA based positioning technology for NB-IoT devices, which is one part of the 3rd Generation Partnership Project (3GPP) Long Term Evolution (LTE). Our thesis work aims at finding a novel algorithm(s) which will help to enhance the positioning accuracies of NB-IoT devices. MATLAB is used as the software to build a link level simulation platform such that the performance of the suggested algorithm(s) can be evaluated. Key elements of our implementation are generating the Positioning Reference Signal (PRS), defining the transmitter specifications, adding channel effect, combining signals at receiver side then at the end estimating the position.

The outline of this thesis is as follow:

Chapter 2 gives a brief theory introduction of NB-IoT and needed background information.

Chapter 3 explains OTDOA positioning method for NB-IoT according to 3GPP standardization with some essentials such as PRS covered in details.

Chapter 4 introduces reference signal design and configuration.

Chapter 5 presents the channel effect and various parts of receiver operation.

Chapter 6 displays different simulation results where our new algorithms are evaluated.

Chapter 7 summarizes the thesis work and outline future work.

2.1 The Internet of Things

3GPP standardization has defined cellular IoT specifications as one of the key enablers for global deployment of IoT. It provides an idea of how the future world looks like and refers to an advanced network which establishes connections of massive number of devices used in our daily life. IoT applications cover a wide range of use cases, including smart cities, smart houses, health-care, automotive and a lot others [5]. It is estimated that billions of IoT devices will be connected to the network by 2025 [6], [7]. With this huge number of connected end user devices, plenty of efforts have been dedicated during 3GPP release 13 to develop cellular technologies that can provide seamless IoT connectivity. Two technologies have risen to the surface to provide connectivity for such huge number of connected nodes. Long-Term Evolution Machine Type Communication (LTE-M) is the another technology that uses a system bandwidth of 1.4MHz. Narrowband IoT (NB-IoT) is the main radio technology covered in this thesis which uses even a smaller bandwidth of 180KHz providing flexible deployment options based on its narrow spectrum [8].

Both technologies can provide reliable communication under severe coverage conditions and support long battery lifetime for many years with the use of low complexity and low cost devices. However, there are other competitive communication standards besides 3GPP looking into IoT and targeting the unlicensed spectrum bands such as Personal Area Networks (PAN), e.g. Bluetooth and ZigBee, and Low Power Wide Area Network (LPWAN)[9]. Each one of the technologies has its own pros and cons but all aim at serving an enormous number of IoT devices.

2.2 NB-IoT

Narrowband-Internet of Things (NB-IoT) is a promising cellular technology that was introduced in 3GPP Release 13. It is developed to provide connectivity for a wide range of new IoT devices. NB-IoT significantly improves the power consumption of user devices, by lowering down the sampling rate [9]. Although NB-IoT is a newly proposed technology, it is still fairly dependent on LTE standard and can therefore co-exist with LTE networks which allow for easy rollout. NB-IoT uses a bandwidth of 180kHz which helps to provide more flexible deployment options. Many LTE aspects have been reused such as modulation schemes, channel coding, and so on [10]. NB-IoT can co-exist inside an LTE network in either in-band mode or guard-band mode. In-band mode is implemented by replacing one of the existing LTE Physical Resource Blocks (PRB) while guard-band mode by deploying it in LTE guard-band. Another operation mode is possible as well by replacing an existing GSM carrier in what is renowned as standalone mode. These three different modes are illustrated in Fig.2.1. Nevertheless, not all LTE functions can be re-used in NB-IoT, since NB-IoT requires less device complexity and lower cost.

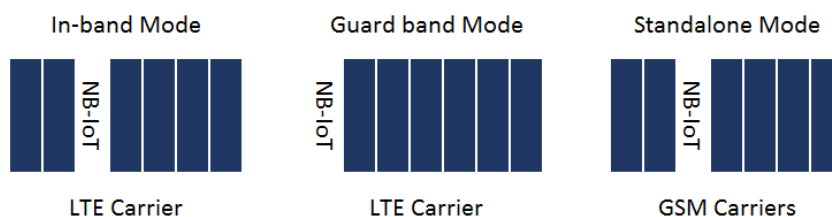


Figure 2.1: NB-IoT Deployment Scenarios

There are several characteristics of NB-IoT that grant it an advantage over other cellular technologies for Massive IoT deployments [1] [11]. Firstly, extended coverage for deep indoor and underground users is supported, based on the fact that NB-IoT operates with 20dB higher Maximum Coupling Loss (MCL) compared to LTE. MCL is normally used to define service coverage since it is the maximum signal attenuation supported by the system for a certain requirement of service delivery. Moreover, lower data rate requirements make it suitable for low complexity UE and low power consumption that leads to an extended battery lifetime. Furthermore, capacity enhancements can be achieved since NB-IoT base stations are expected to support an enormous number of nodes per sector.

In the last 3GPP release 14, several features and enhancements are introduced to NB-IoT. One of the new features that have been added to NB-IoT is the support of device positioning using Observed Time Difference of Arrival (OTDOA), which will be introduced in more details in the next chapter.

2.3 NB-IoT Frame Structure

The NB-IoT radio access technology is mainly based on existing LTE specifications, as a result, NB-IoT shares the same basic terminologies as LTE, such as the time-frequency resource grid [8][9]. As can be seen in Fig.2.2, time-frequency resource grid is represented by 14 Orthogonal Frequency Division Multiplexing (OFDM) symbols in case of normal Cyclic Prefix (CP) configuration. Each symbol consists of 12 subcarriers in the frequency domain with a total bandwidth of 180kHz. All OFDM symbols have fixed length transmission time and summed to a total of 1ms. The transmitted data mapped to the smallest unit of the resource grid known as resource element (RE) illustrated in Fig.2.2, which is uniquely identifiable by subcarrier index k and OFDM symbol index l . In the time domain, each 7 OFDM symbols represents a slot of 0.5ms duration with 2 slots added up to form a single subframe, and 10 subframes are summed up to implement one radio frame of 10ms duration. Each 12 subcarriers and 7 OFDM symbols gather to form a physical resource block (PRB) where a pair of PRBs is the smallest scheduled unit in most of DL cases [9].

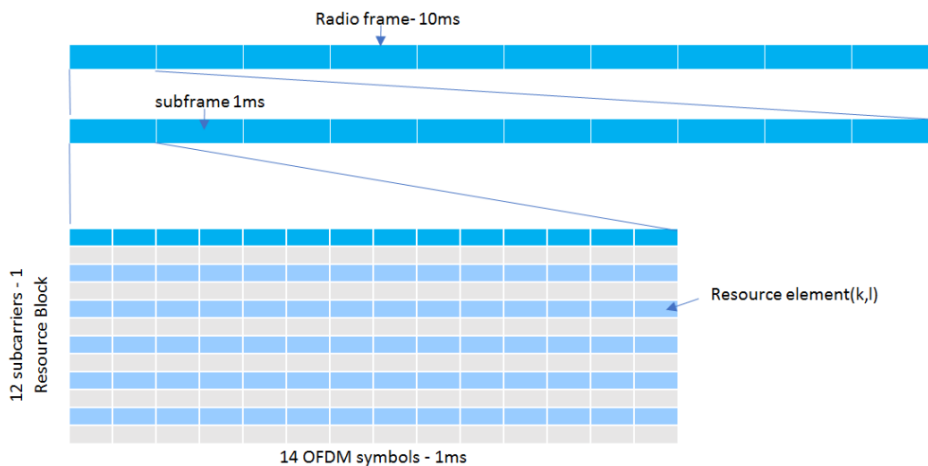


Figure 2.2: LTE Resource Grid

2.4 OFDM Transmission

OFDM is a multicarrier transmission scheme where many narrow-band orthogonal sub-carriers are used to transmit digital symbols over a radio channel. Thus, OFDM can be considered as a combination of both modulation (sending certain data using a certain frequency carrier) and multiplexing (from the fact of combining several sub-carriers). The symbols used will be originally modulated with any conventional modulation scheme (such as QPSK, M -QAM, etc.).

Simple OFDM system can be implemented as in Fig.2.3. To illustrate the structure, let's consider a set of complex modulated symbols $X[k]$ where k ranges from 0 to $N_{sc}-1$ and N_{sc}

symbolizes the number of orthogonal subcarriers (e.g., the IFFT size, 2048 in LTE 20MHz while 128 in NB-IoT) and k denotes the subcarrier index. The output of the IFFT block is $x[n]$ that represents the discrete time version of an OFDM signal which can be generated by applying DFT to the frequency domain symbol $X[k]$.

$$x(n) = \frac{1}{\sqrt{N_{sc}}}x(nT_s) = \frac{1}{\sqrt{N_{sc}}} \sum_{k=0}^{N_{sc}-1} X(k)e^{j2\pi kn} \quad (2.1)$$

Where T_s is the sampling time $T_s = 1/F_s = 1/(N_{sc}\Delta f)$; F_s denotes the sampling frequency; Δf expresses the frequency spacing between two subcarriers; $X[k]$ represents the complex symbols; N_{sc} stands for subcarrier number. The last block of OFDM transmitter is Cyclic Prefix (CP) insertion which has a duration denoted as T_{cp} . It is simply implemented by copying the last portion of the OFDM symbol and appending it prior to the start of the symbol. CP plays a major role as a guard interval and helps to preserve the orthogonality between OFDM symbols in a multi-path environment. Despite the fact that OFDM has a lot of advantages such as higher spectral efficiency and immunity against inter-symbol interference (ISI), it still has some drawbacks compared to single carrier(SC) systems, such as strict synchronization requirements and large Peak to Average Power Ratio (PAPR) which tends to reduce the efficiency of radio frequency amplifiers [12].

Sampling frequency is a variable parameter and it is based on the available bandwidth reflecting the FFT size in use. NB-IoT has a sampling frequency of 1.92MHz which corresponds to FFT size of 128. Additionally, NB-IoT uses the normal CP duration of $4.7\mu s$ except for the first OFDM symbol ($5.1\mu s$). However, the low sampling frequency of NB-IoT has a severe effect on positioning accuracy as will be discussed later on.

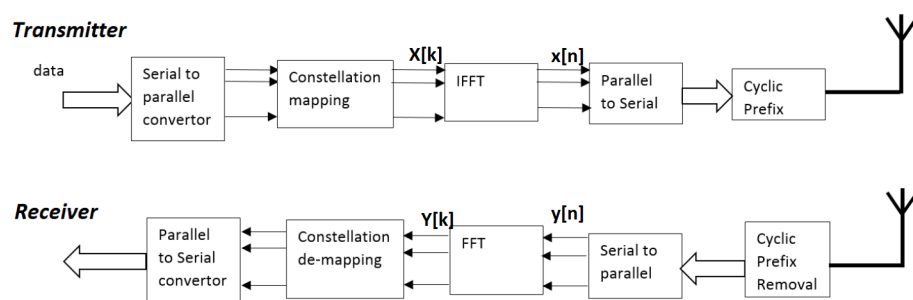


Figure 2.3: OFDM Wireless System Structure

OTDOA POSITIONING

3.1 Introduction

Navigation and positioning are necessary parts of our daily life and the demand on positioning accuracy is becoming more important day by day. Positioning enhancements are mainly achieved by GNSS. With the advances in GNSS receiver designs, it becomes possible to integrate the GNSS system into small portable devices such as mobile phones. However, the performance of GNSS is severely degraded in extreme coverage locations (e.g. urban environment, indoors or underground). In such circumstances, signal propagation is disturbed by the presence of obstacles added to shadowing to an extent that no clear line of sight communication is possible which highly affects GNSS performance. With the increased popularity of wireless devices, such as mobile phones, in the last decades, several technologies and innovations have been proposed to supplement the operation of GNSS in cellular technologies.

With the rapid deployments of wireless networks, the demand of mobile positioning services is increasing dramatically driven by commercial services and applications, it even becomes indispensable in some occasions such as emergency situations [13] [14]. Accordingly, there are a number of methods developed in cellular technologies for positioning estimation where the whole network as well as the end user can benefit from. Some location-based services (LBS) require accurate position estimations which demand the assistance of satellite signals. However, for other services positioning estimation accuracy is not essential, consequently, methods based on cellular estimation is sufficient to be used. The most common cellular positioning methods include, Cell ID method which is the simplest and least accurate one. Estimation based on user equipment's range measurements such as Time of Arrival (TOA) and received signal strength (RSS) which provides improved accuracy over Cell ID method. Other alternatives procedures

exist as well like time difference of arrival (TDOA) and angle of arrival (AOA) [14] that are based on multi-measurements processing.

In 3GPP standard, three different techniques for positioning estimation are supported and each has its own requirements and accuracy. Firstly, Assisted Global Navigation Satellite System (A-GNSS) is a system where cellular networks used to provide data to assist the operation of GNSS receivers. Regardless of this method accuracies, it might be challenging to work properly in many IoT use-cases, especially in severe indoor radio conditions [4]. Secondly, Enhanced Cell ID (E-CID) is a localization procedure where the device position is estimated using the serving cell ID and UE measurements, including data such as Round Trip Time (RTT) and many others as can be seen in [15], [14], [16]. Finally, OTDOA that represents the scope of this thesis and will be described in more details in the incoming sections.

3.2 OTDOA positioning

OTDOA is a downlink (DL) based positioning method with its basic principle as shown in Fig.3.1. The procedure of OTDOA can be summarized as follows: firstly, several synchronized eNBs simultaneously transmit the PRSs (Positioning Reference signal) which are received by the UEs. Then, the UEs estimate the time of arrival (TOA) of signals received from multiple eNBs. After that, OTDOAs are formed by analyzing the differences between the arrival time instances. Afterwards, UE positions can be found by calculating the intersections of the hyperbolas created by each time differences. A minimum of three eNBs are required to obtain an accurate result and eNBs exact locations information are also necessary [4], [15], [2]. OTDOA positioning accuracy is heavily dependent on the environment radio conditions.

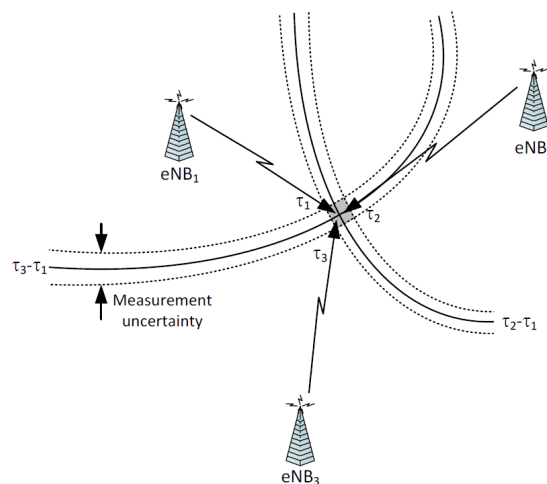


Figure 3.1: OTDOA Basic Principle [2]

Two different variants of positioning procedure may take place either in control plane, or user plane. LTE Positioning Protocol (LPP) is clarified in Fig.3.2. The complete detailed general procedure is specified in LTE positioning protocol [15]. As a summary, in control plane variant, the network initiates the positioning procedure on behalf of a target UE where all OTDOA assistance data and signals are carried over control channels. Likewise, in user plane similar functionality is followed but signaling information will be sent on data bearers with other user data.

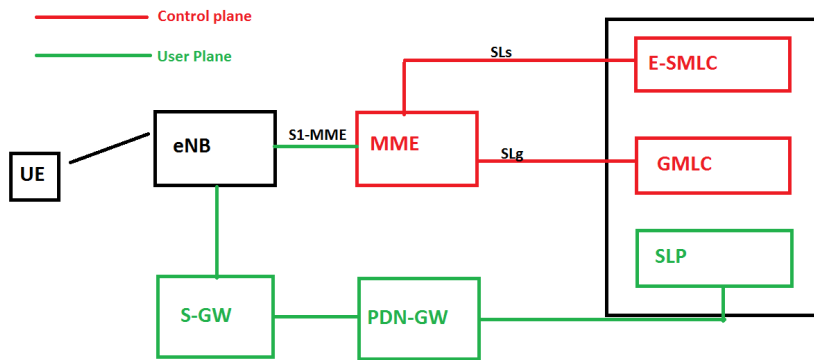


Figure 3.2: LTE Location Service Architecture [2]

3.3 Positioning Procedure

NB-IoT positioning is also based on LPP protocol. LPP protocol procedures consist of the following steps[15]:

1) **Capability Transfer:** where the server sends a “RequestCapabilities” message to the UE which replies by a “ProvideCapabilities” message including OTDOA related parameters (e.g. frequency bands supported or OTDOA mode supported).

2) **Assistance Data Transfer:** in which the UE sends a “RequestAssistanceData” message to the server that responds with supplying OTDOA assistance data with a “ProvideAssistanceData” message.

3) **Location Information Transfer:** here the server requests UE location information which then performs TOA measurements and updates the server with the data before the expiry of the maximum response timer. For more details regarding the LPP, interested readers may refer to 3GPP standard dedicated to LTE positioning procedure [15].

3.4 Narrowband Positioning Reference Signal (NPRS)

Reference signals mainly used for data synchronization, such as Primary Synchronization Signal (PSS) and Secondary Synchronization Signal (SSS), besides channel estimation. 3GPP introduced

as well Narrowband positioning reference signals (NPRSs) used to enable OTDOA positioning. NPRS is mainly used by the UE to estimate different time of arrivals from signals transmitted via multiple base stations, such that the estimated position can be obtained. NPRS is defined in 3GPP TS 36.211 [8] carried on NB-IoT resource Blocks which configured for NPRS transmission. NPRS signals are mapped to different REs consisting of Quadrature Phase Shift Keying (QPSK) modulated generated random sequences using same sequence generator. However, each generated sequence is unique because it is based on slot number, cell ID, OFDM symbol and CP type. The NPRS sequence $Z_{n_s,l}$ is defined by

$$z_{n_s,l}(m) = \frac{1}{\sqrt{2}}(1 - 2c(2m)) + j\frac{1}{\sqrt{2}}(1 - 2c(2m + 1)) \quad (3.1)$$

where n_s represents the symbol number, l the slot number, $m \in \{0, 1\}$ and $c(m)$ is 31 length Gold sequence initiated with the seed

$$c_{init} = 2^{28} \left\lfloor \frac{N_{ID}}{512} \right\rfloor + 2^{10}(7(n_s + 1) + l + 1)(2(N_{ID} \bmod 512) + 1) + 2(N_{ID} \bmod 512) + N_{CP} \quad (3.2)$$

where N_{ID} is denoted as PCI of the eNB, N_{CP} represents the CP and it is equal to 1 for normal CP and zero for extended CP.

The idea behind using Gold codes to initiate NPRS is because of its good correlation properties since gold codes demonstrate good auto correlation and low cross correlation with codes initiated from different seeds. Such properties will assist NPRS to be detected using simple correlator suitable for NB-IoT devices.

According to equation 3.4, NPRS introduces a frequency reuse factor of six based on cell identity value which means that v_{shift} holds values from 0 to 5 based on cell ID and allows six different cells to transmit NPRS signals in different subcarriers. NPRS mapping to REs is shown in Fig.3.3 which illustrates different settings of NB-IoT operating in standalone mode compared to in-band mode. In Fig.3.3, R_0 and R_6 stand for antenna port 0 and 6 respectively. In general, the reference signal sequence $z_{n_s,l}(m)$ is mapped to complex-valued modulation symbol $a_{k,l}^p = z_{n_s,l}(m)$ where p represents the antenna port, $k = 6m + (6 - l + v_{shift}) \bmod 6$ and $m = 0, 1$.

For in-band mode,

$$k = \begin{cases} 3, 5, 6 & n_s \bmod 2 = 0 \\ 1, 2, 3, 5, 6 & n_s \bmod 2 = 1 \end{cases} \quad (3.3)$$

$$v_{shift} = N_{ID} \bmod 6 \quad (3.4)$$

This corresponds to a total of 8 symbols in in-band mode being allocated for NPRS transmission. Other symbols are utilized by LTE reference signals and control channels (e.g. Physical Broadcast Channel, PBCH), while for standalone implementation all of the symbols will be utilized by NPRS.

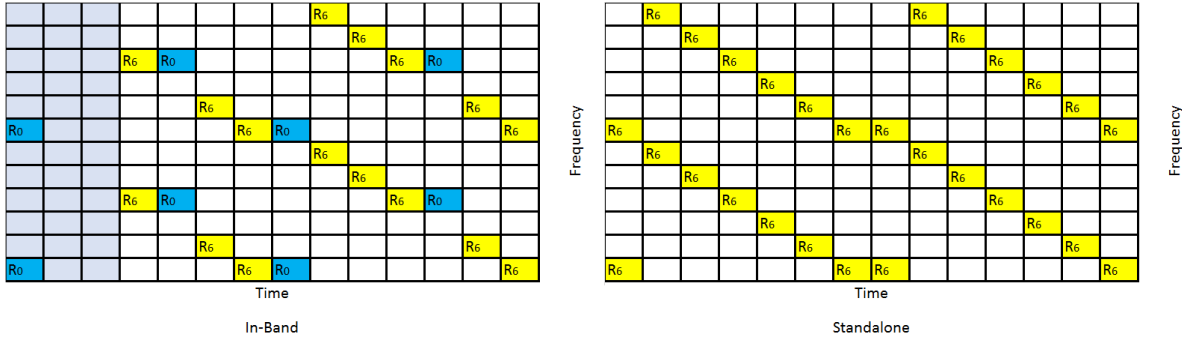


Figure 3.3: NPRS Mapping to Resource Elements

3.5 Reference Signal Time Difference (RSTD) measurement

RSTD is the measurement done by UE for OTDOA positioning and it is specified in 3GPP TS 36.214 [17]. RSTD is defined as the relative timing difference between two cells , reference cell and measured one, calculated as

$$RSTD = T_{subframeRxj} - T_{subframeRxi} \quad (3.5)$$

where $T_{SubframeRxj}$ corresponds to the time the UE receives a start of subframe from cell j and $T_{SubframeRxi}$ represents to the time the UE receives a start of subframe from cell i.

The reference point for OTDOA is selected by the UE. And the eNBs need to be synchronized, so the PRS occasions of all eNBs are aligned in time. RSTD measurement is possible on either intra-frequency (when both cells i and j belongs to the same carrier frequency) or inter-frequency (when both cells belong to different carrier frequencies). More information and details which beyond the scope of this thesis work related to RSTD measurements reporting and RSTD search window can be found in [15], [17], [18].

3.6 Time of Arrival (TOA)

In a wireless system, the distance between the transmitter and receiver can be easily estimated by measuring the propagation time between the two nodes with the knowledge of speed of light. For instance, let's assume a simple ideal system where we have two nodes communicating as in figure 3.4 with perfect clock synchronization. Moreover, suppose that the transmission time is embedded into the transmitted signal (T_{Tx}) such that once the receiver estimates the arrival time (T_{Rx}), the distance can be easily calculated as follows:

$$D = (T_{Rx} - T_{Tx}) * c \quad (3.6)$$

However, to achieve a perfect network synchronization is a challenging task, which results in inaccurate TOA estimations to some extent. Additionally, radio propagation environment will

have a huge impact on TOA estimation due to multipath and scattering effects. To overcome the previous drawback, GPS receivers are used in real life networks to guarantee the clock synchronization as well as channel equalization and advanced receiver algorithms are implemented to overcome the channel effect. Correlator can be considered as the simplest TOA estimator, which will be covered in Chapter 5.

3.7 Time Difference of Arrival (TDOA)

TDOA estimation is an essential step in multiple applications, such as positioning, where the performance accuracy is linked to the accuracy of TDOA estimations. In this algorithm, the receiver measures the TOA from all the transmitting nodes then the difference of time of arrival for all the possible couple of measurements will be evaluated. Based on the results, the receiver position can be estimated. TDOA measurements represent the basis for the so-called OTDOA algorithm introduced in Section 3.2.

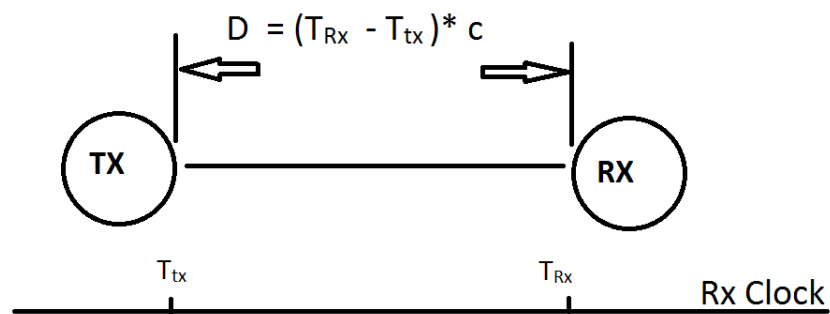


Figure 3.4: TOA Principle

DESIGN OF REFERENCE SIGNAL AND CONFIGURATION

In this chapter, design of positioning reference signal and configuration will be introduced. Initially, a base link level simulation has been implemented which helped to simulate and evaluate the current NB-IoT in-band OTDOA positioning standard, then it has been expanded to cover the scope of our thesis work. A generalized transmission of positioning reference signal procedure is summarized in the block diagram shown in Fig.4.1. The procedure starts by choosing which sequence to be configured by the eNB (different sequences have been tested out, which will be introduced in Section 4.4). After that, we initiate our PRS (M -PSK or M -QAM) symbols generated from the chosen sequence followed by mapping to the time-frequency resource grid. The next step is to simulate either NB-IoT by sending a single PRB per subframe or beyond NB-IoT (higher bandwidth settings) by assigning more than one PRB to a single subframe. OFDM symbol is created by IFFT operation and cyclic prefix addition. Finally, either one or multiple subframes is(are) transmitted and processed by the receiver. The rest of Chapter 4 includes the detailed transmitter configuration schemes and it is structured as follows: *Increasing PRS Density (Section 4.1)*, *Different 2 PRS Designs (Section 4.2)*, *Optimizing the Original Gold Sequence (Section 4.3)*, *PRS Initialization Based on Different Sequences (Section 4.4)* and *Sending Multiple Subframes and/or PRB's (Section 4.5)*.

4.1 PRS Density

As previously introduced in Chapter 3, where a single cell ID mapped to REs, a generalized time-frequency grid of 6 different cell ID's is as shown in Fig.4.2 in accordance with [8]. Based on the relevant frequency-time relationship, the transmitted signal will get a narrower main-lobe of its autocorrelation function if the signal occupies more subcarriers (increased BW) in the frequency domain. Here, we propose new time-frequency grids, which utilize more subcarriers

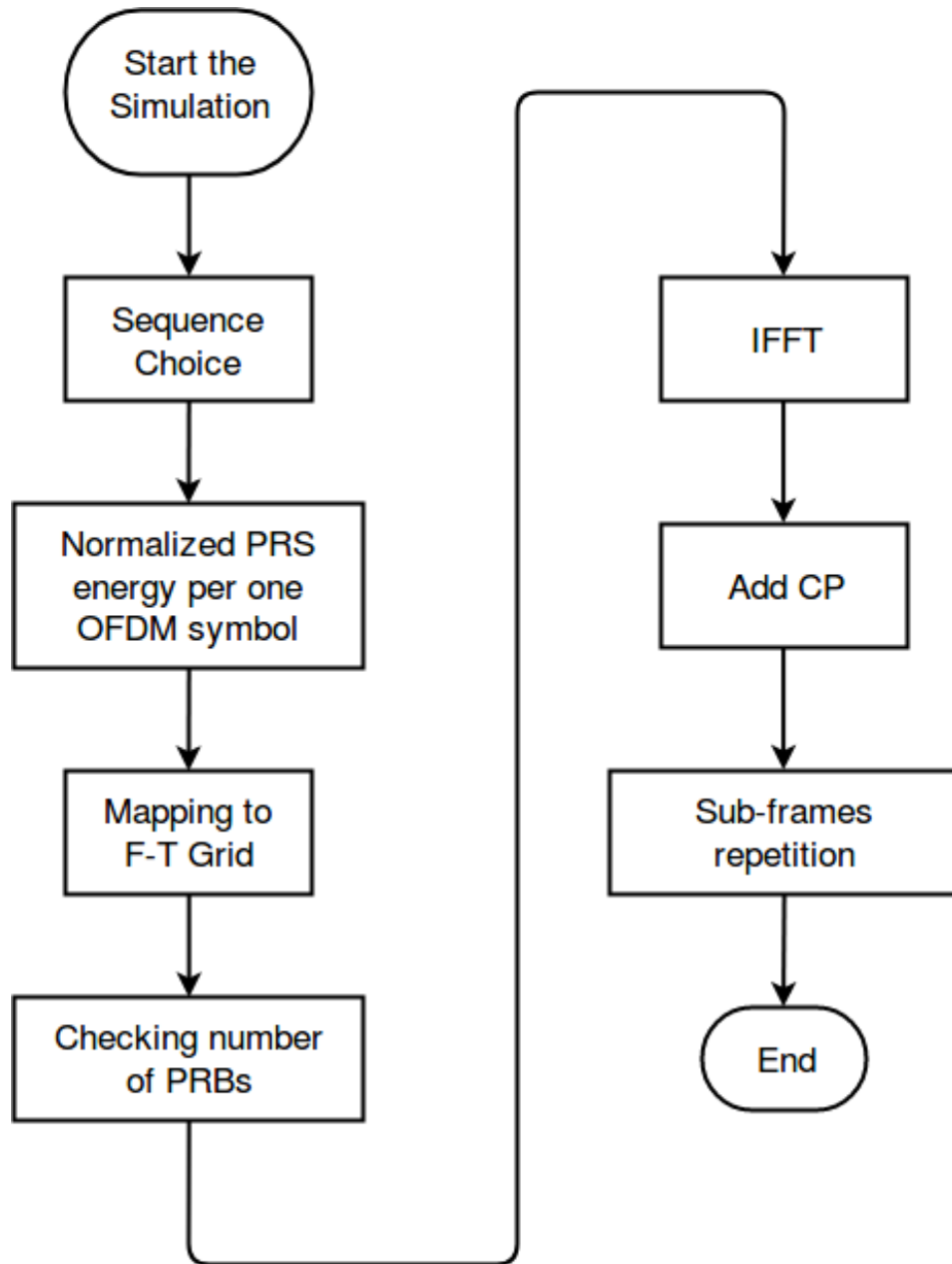


Figure 4.1: Tx Process

per eNB in a single OFDM symbol. The two suggested designs are based on changing the original v_{shift} value in equation 3.4. The new suggested v_{shift} corresponding to 3PRS and 4PRS designs are given by equations 4.1 and 4.2 respectively.

$$v_{shift} = N_{ID} \bmod 4 \quad (4.1)$$

$$v_{shift} = N_{ID} \bmod 3 \quad (4.2)$$

The NPRS sequence $Z_{n_s,l}$ is defined as below for 3 NPRS design

$$Z_{n_s,l}(m) = \frac{1}{\sqrt{3}}(1 - 2c(2m)) + j\frac{1}{\sqrt{3}}(1 - 2c(2m + 1)) \quad (4.3)$$

where n_s represents the symbol number, l the slot number, $m \in \{0, 1, 2\}$ and $c(m)$ is 31 length gold sequence initiated with the same seed as equation 3.2 and $k = 4m + (4 - l + v_{shift}) \bmod 4$. While for 4 NPRS design the NPRS sequence $Z_{n_s,l}$ is defined by

$$Z_{n_s,l}(m) = \frac{1}{2}(1 - 2c(2m)) + j\frac{1}{2}(1 - 2c(2m + 1)) \quad (4.4)$$

where n_s represents the symbol number, l the slot number, $m \in \{0, 1, 2, 3\}$ initiated with the same seed and $k = 3m + (3 - l + v_{shift}) \bmod 3$.

The suggested two grid designs are shown in Fig.4.3 & Fig.4.4.

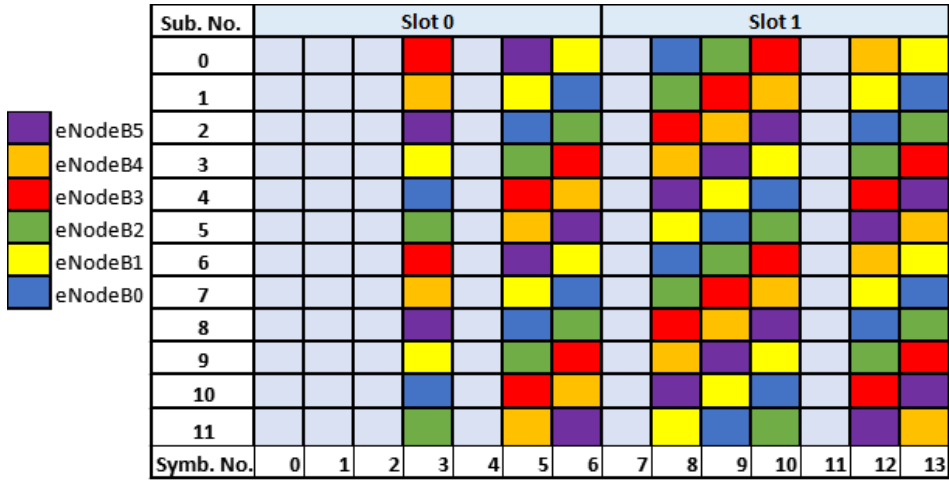


Figure 4.2: Original Resource Grid

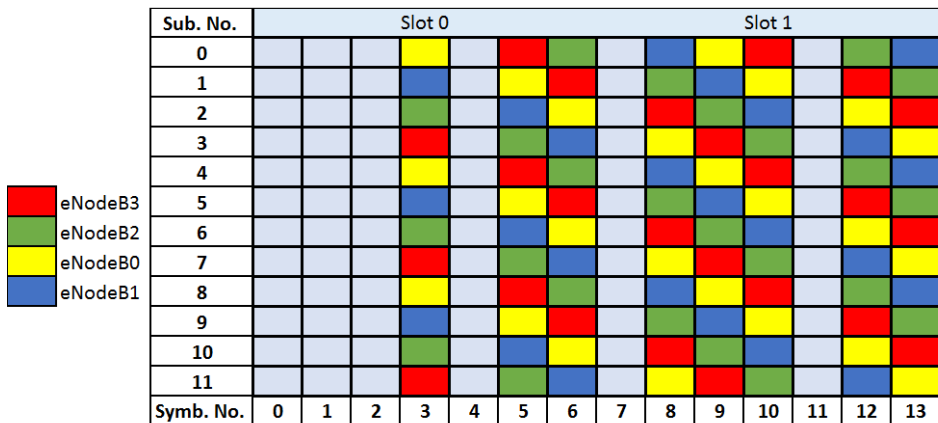


Figure 4.3: Three PRSs Resource Grid

Compared the proposed designs with the standard, increasing the PRS density from 2 subcarriers to 3 or 4 per a single OFDM symbol reduces the total number of supported eNBs

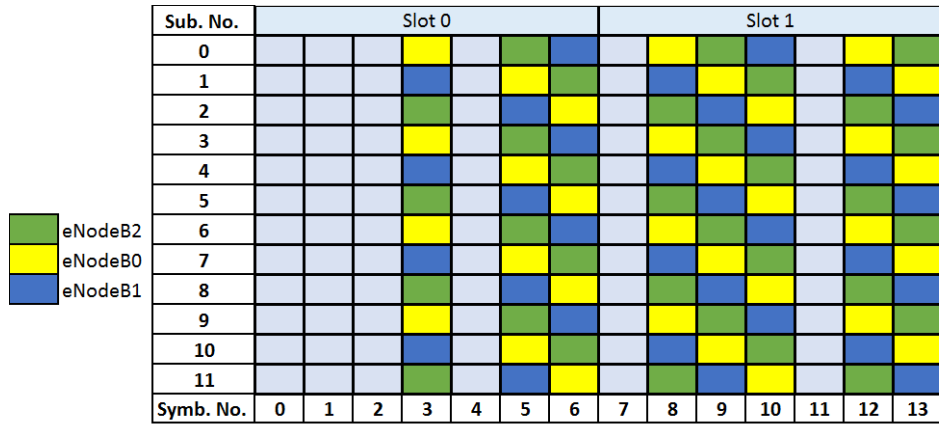


Figure 4.4: Four PRSs Resource Grid

in a single PRB from 6 to 4 or 3 subsequently. In order to ensure that the autocorrelation functions for all eNBs at transmitter side with the newly proposed schemes are similar, the frequency separations between the PRS subcarriers belong to the same eNB under one OFDM symbol are equivalent to each other. Our proposed schemes can achieve the benefit of a narrower autocorrelation main-lobe, as depicted in Figs.4.5 and 4.6. However, the tradeoff of such designs is clearly the increase of inter-cell interference between eNBs which result in worse performance of positioning accuracy with increased number of eNBs more than 4.

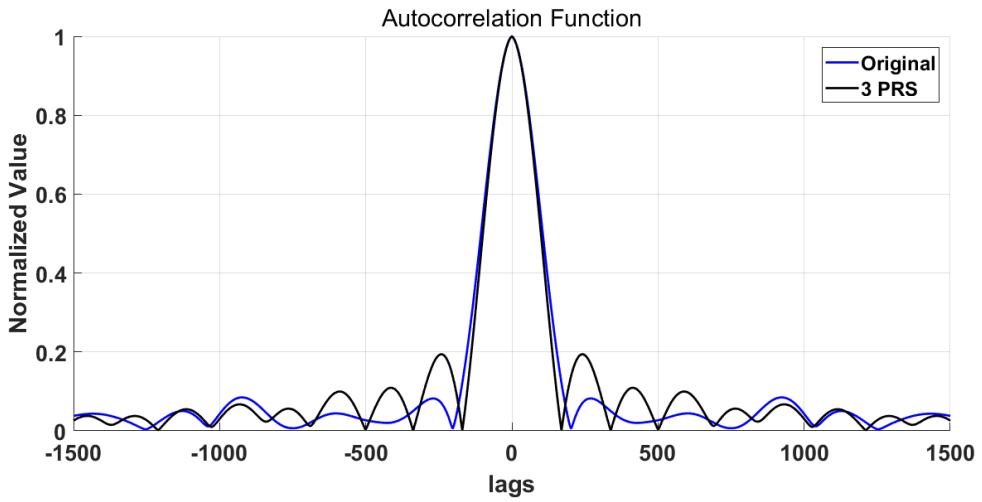


Figure 4.5: AutoCorrelation of 3PRS vs Original

4.2 Different Time Frequency Resource Block Designs

In this section, our main focus is to change the original 2 PRS design using the same density (2 PRS signals for each eNB under a single OFDM symbol) but with different subcarrier assignments.

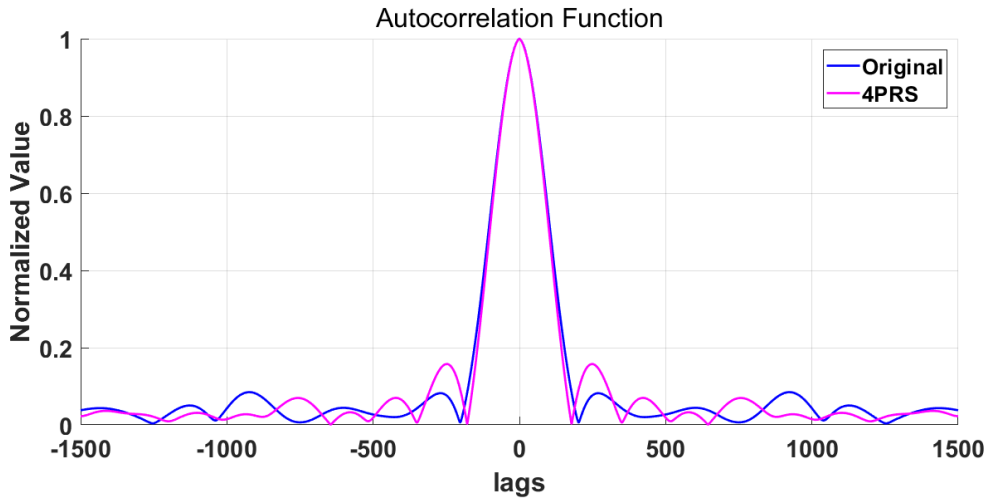


Figure 4.6: AutoCorrelation of 4PRS vs Original

Here, we propose 4 different designs under the framework of 6 eNBs within a resource grid. In chapter 6, the performance of different designs will be tested out against the original one.

4.2.1 Proposed Design Scheme 1

By recalling the standard resource grid shown in Fig.4.2, it is clear that some frequency subcarriers are not fairly distributed among all eNBs (such as subcarrier number 2, it doesn't carry NPRS for eNB1). Therefore, in order to efficiently spread the subcarriers equally across all eNBs (each subcarrier is utilized by each eNB), we propose a new design, which is illustrated in Fig.4.7. Compared with the standard grid design, the newly proposed one fairly utilizes the subcarriers across all eNBs to a better extent. To guarantee that the autocorrelation of the transmitted signals is similar across all eNBs, the frequency separation is maintained identical. Autocorrelation of such frequency assignment is shown in Fig.4.8.

Sub. No.	Slot 0						Slot 1							
0				Yellow		Purple	Red	Green	Blue		Yellow	Purple		
1				Blue		Yellow	Yellow	Red	Green		Blue	Yellow		
2				Green		Blue	Purple	Yellow	Red		Green	Blue		
3				Red		Green	Yellow	Purple	Blue		Red	Green		
4				Yellow		Red	Blue	Yellow	Purple		Yellow	Red		
5				Purple		Yellow	Green	Blue	Yellow		Purple	Yellow		
6				Yellow		Purple	Red	Green	Blue		Yellow	Purple		
7				Blue		Yellow	Yellow	Red	Green		Blue	Yellow		
8				Green		Blue	Purple	Yellow	Red		Green	Blue		
9				Red		Green	Yellow	Purple	Blue		Red	Green		
10				Yellow		Red	Blue	Yellow	Purple		Yellow	Red		
11				Purple		Yellow	Green	Blue	Yellow		Purple	Yellow		
Symb. No.	0	1	2	3	4	5	6	7	8	9	10	11	12	13

Figure 4.7: Resource Grid Design 1

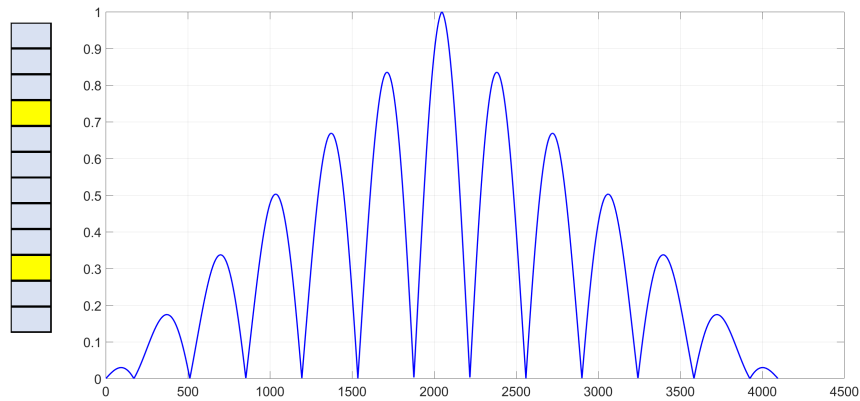


Figure 4.8: Normalized ACF of 6 sub-carriers Spacing

4.2.2 Proposed Design Scheme 2

As illustrated by the standard and the previously proposed resource grids, the frequency separation in a single OFDM symbol between two different subcarriers reserved by each eNB remains constant throughout the whole resource grid. For another design proposal shown in Fig.4.9, we decided to test the effect of changing the frequency separation between subcarriers. The main characteristic of this scheme is that for every eNB, there exists at least one (or two) symbol achieving the maximum frequency separation, resulting in the narrowest autocorrelation function but with the highest effective side lobes. However, there also exists at least one (or two) symbol with subcarriers belong to the same eNB right next to each other, leading to the widest ACF instead without sidelobes.

Sub. No.	Slot 0						Slot 1							
0				Yellow		Purple	Orange		Red	Green	Blue		Yellow	Purple
1				Blue		Yellow	Purple		Orange	Red	Green		Blue	Yellow
2				Green		Blue	Yellow		Purple	Orange	Red		Green	Blue
3				Red		Green	Blue		Yellow	Purple	Orange		Red	Green
4				Orange		Red	Green		Blue	Yellow	Purple		Orange	Red
5				Purple		Orange	Red		Green	Blue	Yellow		Purple	Orange
6				Blue		Yellow	Purple		Orange	Red	Green		Blue	Yellow
7				Yellow		Blue	Green		Red	Purple	Orange		Yellow	Blue
8				Red		Blue	Yellow		Purple	Orange	Red		Green	Blue
9				Green		Yellow	Purple		Orange	Red	Blue		Green	Yellow
10				Blue		Yellow	Purple		Orange	Red	Green		Blue	Yellow
11				Yellow		Purple	Orange		Red	Green	Blue		Yellow	Purple
Symb. No.	0	1	2	3	4	5	6	7	8	9	10	11	12	13

Figure 4.9: Resource Grid Design 2

In Fig.4.10, a sample of ACF for different PRS symbols of design 2 is provided.

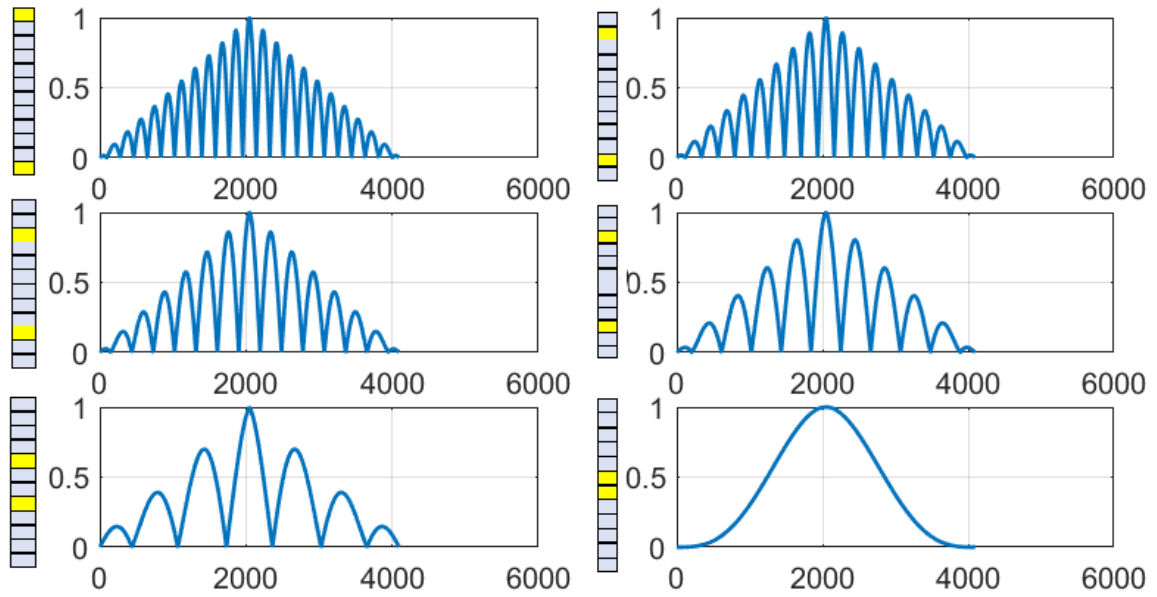


Figure 4.10: ACF of different sub-carriers Spacing

4.2.3 Proposed Design Scheme 3

Since at least one or two symbols in our second suggested design gives wider autocorrelation main-lobe while others result with the narrowest autocorrelation possible, therefore, we propose another design scheme as illustrated in Fig.4.11. In this design scheme, we aim to tune the ACF of the eNBs under a single OFDM symbol by keeping the assignment achieves the highest frequency separation (PRS are far from each other) while avoiding the adjacent subcarriers deployment.

Sub. No.	Slot 0						Slot 1							
0				Yellow				Red	Orange	Purple		Yellow	Blue	
1				Blue		Green		Red	Purple			Blue	Green	
2				Purple		Yellow		Green	Red	Orange		Purple	Yellow	
3				Orange		Purple		Blue	Green	Red		Orange	Purple	
4				Green		Red		Yellow	Blue	Green		Red	Orange	
5				Red		Orange		Purple	Yellow	Blue		Red	Orange	
6				Purple		Yellow		Green	Red	Orange		Purple	Yellow	
7				Orange		Purple		Blue	Green	Red		Orange	Purple	
8				Green		Red		Yellow	Blue	Green		Red	Orange	
9				Red		Orange		Purple	Yellow	Blue		Red	Orange	
10				Blue		Green		Orange	Purple	Yellow		Blue	Green	
11				Yellow		Blue		Red	Orange	Purple		Yellow	Blue	
Symb. No.	0	1	2	3	4	5	6	7	8	9	10	11	12	13

Figure 4.11: Resource Grid Design 3

4.2.4 Proposed Design Scheme 4

In our last proposed design which is given by Fig.4.12. Based on this scheme, for each eNB one or two symbols achieve the maximum frequency separation. For other symbols the distance between different PRSs under one symbol belongs to the same eNB remains constant. As an example, checking the first symbol configuration, we can see that for the first eNB (represented by yellow), PRS separation is maximized while for remaining eNBs, the separation is the same and equals to 4.

Sub. No.	Slot 0						Slot 1							
	0				Yellow		Blue	Green		Red	Orange	Purple		Yellow
1				Blue		Green	Red		Orange	Purple	Yellow		Blue	Green
2				Green		Red	Orange		Purple	Yellow	Blue		Green	Red
3				Red		Orange	Purple		Yellow	Blue	Green		Red	Orange
4				Orange		Purple	Yellow		Blue	Green	Red		Orange	Purple
5				Purple		Yellow	Blue		Green	Red	Orange		Purple	Yellow
6				Blue		Green	Red		Orange	Purple	Yellow		Blue	Green
7				Green		Red	Orange		Purple	Yellow	Blue		Green	Red
8				Red		Orange	Purple		Yellow	Blue	Green		Red	Orange
9				Orange		Purple	Yellow		Blue	Green	Red		Orange	Purple
10				Purple		Yellow	Blue		Green	Red	Orange		Purple	Yellow
11				Yellow		Blue	Green		Red	Orange	Purple		Yellow	Blue
Symb. No.	0	1	2	3	4	5	6	7	8	9	10	11	12	13

Figure 4.12: Resource Grid Design 4

4.3 Optimizing the Original Gold Sequence

Another approach applied in our thesis work is a mathematical way to optimize the original gold sequence generated based on cell IDs. To apply this method, two different proposals have been implemented.

- The first proposal targets to narrow the ACF main-lobe of the transmitted signal of a whole resource block that belongs to all eNBs by optimizing the energy distribution of each subcarrier.
- The second approach is based on RE QPSK symbols energy optimization.

Briefly, in the first approach, a single eNB has been considered. In the first stage, a certain eNB (Namely, eNB “0”) has been chosen, then a complete resource block is initiated with the corresponding QPSK symbols of PRS signals. Afterwards, a convex optimization algorithm ¹ is applied and optimized amplitudes have been generated by this algorithm. Lastly, the original

¹Since the mentioned problem needs convex optimization and it does not have a closed-form solution, and to solve it, the built-in function of MATLAB fmincon has been used. The result may not be optimal.

QPSK symbols have been weighted using the generated values by the algorithm. Then similar weighting values have been applied for all other eNBs included in OTDOA positioning process.

In the second approach, as mentioned earlier, each resource element QPSK symbol has been considered independently in the optimization process. Initially, the first symbol belongs to the first eNB has been chosen in frequency domain. Then, the symbol is transferred to time domain for its auto-correlation to be computed. In the following stage, optimization algorithm has been applied to minimize the energy of the auto-correlation main-lobe using the convex optimization method. In the next step, symbol weighting is applied based on the optimization result. Finally, same procedure has been conducted for all the symbols belong to all the eNBs included in OTDOA process.

Briefly, the mathematical process of the optimization algorithm can be presented as follows: Supposing that X is the 12-dimensional vector (where 12 is the total number of subcarriers in an OFDM symbol), A stands for the IDFT matrix of size 2048×12 . After the IDFT process, the signal x is given as:

$$x = AX \quad (4.5)$$

The matrix B is denoted as the autocorrelation matrix, such as

$$B = xx^H \quad (4.6)$$

The peak of the autocorrelation can be calculated as the trace of B since $Tr(B) = Tr(xx^H) = Tr(x^Hx)$. Then, the objective function of the optimization is denoted as

$$J(x) = \sum_{i=1}^{2048} \sum_{j=1, j \neq i}^{2048} |B_{ij}| \quad (4.7)$$

Our task is to minimize the objective function and find the optimal value of x which in itself is a convex optimization problem.

Both methods show good consistent results when applied to certain eNode-Bs configuration. However, such methods consume more computation time in addition to high implementation complexity. As well as, the generated symbols don't have constant amplitudes which make it harder to be mapped to a known conventional modulation scheme. Therefore, to implement such approaches for NB-IoT applications is considered highly challenging.

4.4 Investigation on PRS Sequences

Our next research focus to enhance the positioning accuracy, is to try different sequences instead of the legacy gold sequence for initializing PRS QPSK symbols at the transmitter side. In terms of designing or choosing a new sequence, the following criteria need to be considered:

- Correlation Properties

- Peak to Average Power Ratio
- Positioning Performance
- Flexibility
- Hardware Complexity

The sequences which have been considered in our research include Zadoff-Chu(ZC), Hadamard-Walsh, Zero Cross Correlation complementary (ZCC) sequences, and a novel proposed sequence based on Barker code. Other methods as well have been tested out to minimize cross correlation and maximize auto-correlation, however, they have been dropped-out due to the inferior performance. In the following subsections, details of each sequence will be presented while the simulation results are going to be introduced in Chapter 6.

4.4.1 Zadoff-Chu Sequence

Zadoff-Chu sequence is widely used in LTE due to its decent correlation properties so it can be seen in PRACH preambles, PSS and NSS. It satisfies a Constant Amplitude Zero Autocorrelation (CAZAC) property which allows multiple orthogonal sequences to be generated from the same ZC base sequence [19]. It was developed following correspondences by Frank, Zadoff and Heimiller [20]. Lastly a correspondence by Chu [21] leads to the general form used in NB-IoT.

The ZC sequence of odd-length N_{zc} is given by:

$$A_u = \exp(-j2\pi un(n+1)/N_{zc}) \quad (4.8)$$

where N_{zc} is denoted as the ZC sequence length; u as the root number and n the frequency domain element.

ZC sequences have several important properties include the following [19]:

- Constant amplitude which limits the Peak to Average Power Ratio as well as simplifies the implementation due to the fact that only phases need to be computed, as shown in Fig.4.13.
- 2- ZC sequences have ideal cyclic autocorrelation performance. Autocorrelation of a ZC sequence with length of 839 is shown in Fig.4.14.
- The circular cross-correlation function absolute value between any different two ZC sequences remains constant and equals to $1/\sqrt{N_{zc}}$, provided that $|u_1 - u_2|$ is relatively prime with respect to N_{zc} , where u_1 and u_2 are the sequence indices [19].

The last property can be clarified with the following example, 3 ZC sequences have been generated of length 63 and roots of 25, 29, and 34 used in PSS signaling. By judging whether the difference of two roots of the ZC sequence pair is prime to the length of N_{zc} , we can evaluate the cross-correlation property of the sequence. It can be seen that for the 2 sequences with roots 25

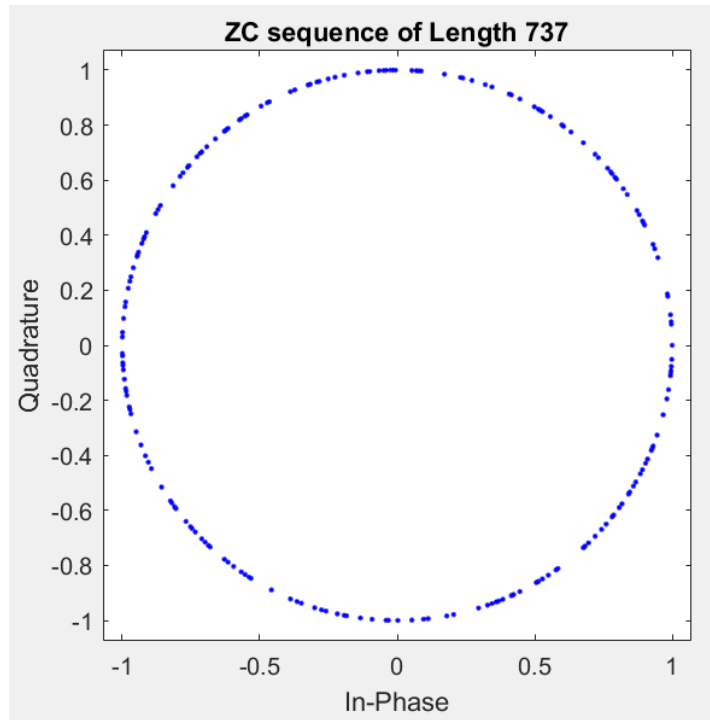


Figure 4.13: ZC Constellation Diagram

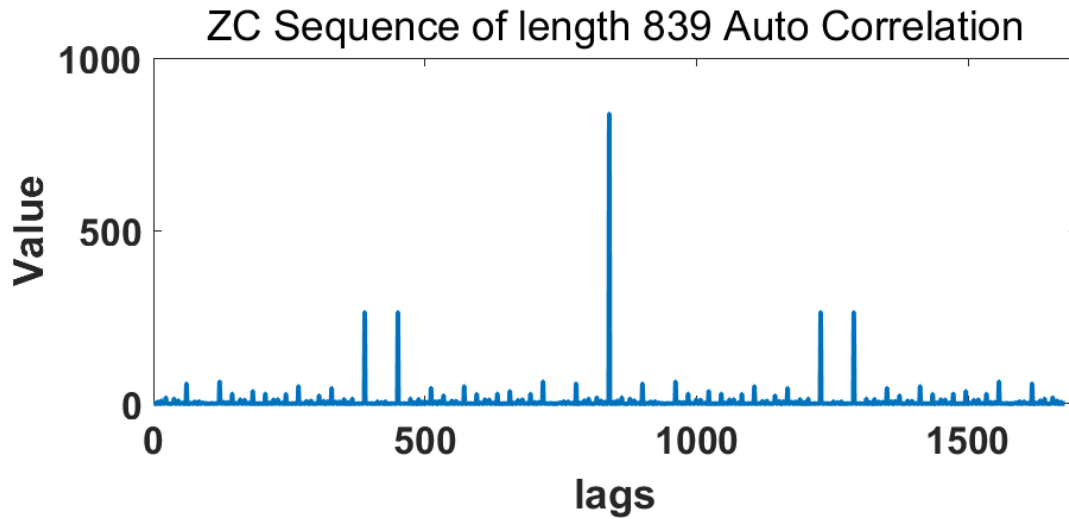


Figure 4.14: ZC sequence of length 839 Autocorrelation

and 29 (4 is prime to 63), the cross correlation has a constant value, almost equivalent to $1/\sqrt{N_{zc}}$. However, for the sequence pair with roots 25 and 34, the difference is not prime to the N_{zc} length (9 not prime to 63), leading to cross correlation values which are not constant. Cross correlation for both illustrated in figure 4.15.

In order to use ZC sequences as positioning reference signals, several aspects need to be taken

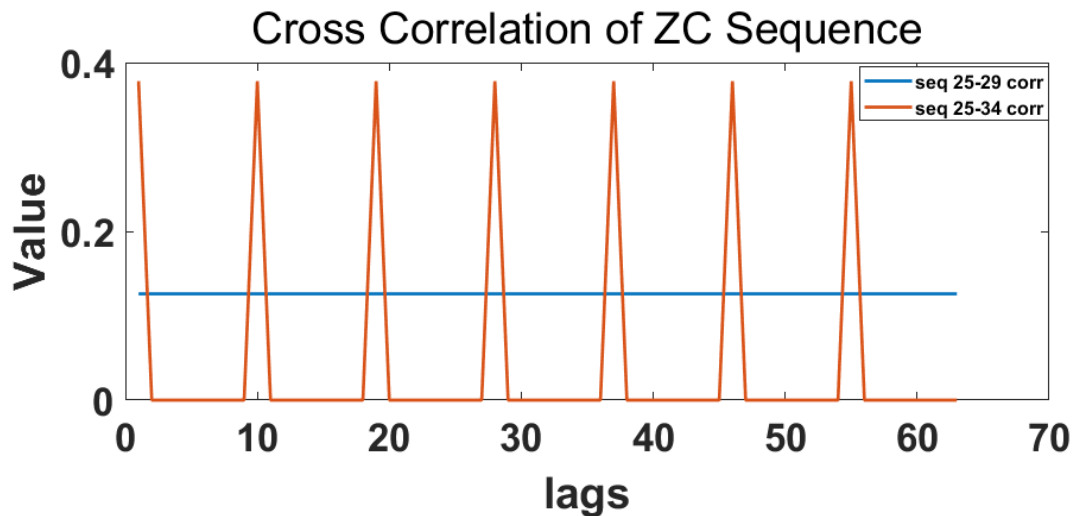


Figure 4.15: Cross Correlation of ZC Sequence of length 63 and roots 25 29 and 34

into consideration.

- ZC Sequence Length
- ZC Root Value
- Mapping ZC Sequence to the REs

For the sake of positioning test, we decided to generate only a small matrix of size 12×6 , derived from a ZC sequence of a certain length. Therefore, we started by ZC sequence length choice and tested out 3 different ZC sequences of lengths (63, 839 and 997). Then we followed the procedure given below to generate our matrices.

- Generate all ZC sequences of a certain length (namely 63, 839, 997), with roots prime to the length.
- Remove the last, first and mid values of each sequence.
- Cascade all of the sequences into a large matrix
- Divide the matrix into blocks of 12×6 . The size constraint is related to the fact that 6 cell IDs can be configured within a resource block and each cell ID needs 12 values in the case of inband mode.
- Test out the auto-correlation properties of each block.
- Keep only the best block in terms of auto correlation and use it as initiation of PRS signals.

Despite the fact that ZC sequences hold good correlation properties, they still less immune to phase shifts introduced by fading channels. Moreover, the QPSK symbols will be no longer conventional since they are derived from M-PSK signal constellation.

4.4.2 Hadamard-Walsh Codes

Walsh codes are orthogonal codes which used in both Second Generation (2G) and Third Generation (3G) cellular radio systems to provide channelization. Walsh codes are found as well in IS-95 Code Division Multiple Access (CDMA) and CDMA-2000 to provide separate channels under the same base station to support multiple users. Walsh codes can be generated by several methods but one famous way derived from Hadamard matrices [22].

The Hadamard matrix is a square array of plus and minus ones, $+1, -1$, whose rows and columns are mutually orthogonal. The Hadamard-Walsh codes are generated in a set of $N = 2^n$ codes with length $N = 2^n$, with the algorithm provided below:

- (1) The first matrix in a Hadamard transform is 2×2 Hadamard matrix of order 2, such as:

$$H_2 = \begin{bmatrix} 1 & 1 \\ 1 & -1 \end{bmatrix}$$

- (2) Then the second matrix can be formed using the first matrix as shown below,

$$H_4 = H_2 \otimes H_2 = \begin{bmatrix} 1 & 1 & 1 & 1 \\ 1 & -1 & 1 & -1 \\ 1 & 1 & -1 & -1 \\ 1 & -1 & -1 & 1 \end{bmatrix}$$

where \otimes is denoted as the Kronecker product.

- (3) Lastly the subsequent matrices can be generated using the below matrix expansion form

$$H_{2N} = \begin{bmatrix} H_N & H_N \\ H_N & \overline{H_N} \end{bmatrix}$$

where $\overline{H_N}$ represents the opposite of matrix H_N .

Each row in Hadamard-Walsh matrix represents a codeword and all the generated codes are orthogonal to each other. Due to orthogonality, the circular cross correlation between any two codes of the matrix is zero but the main problem of such codes comes from the very poor autocorrelation properties [22].

In order to evaluate Walsh codes for positioning, we begin with generating a 16×16 matrix and then truncate it to a 12×6 matrix for the same reason given in the previous section. In the second step, we use the matrix as initialization for the PRSs. As a result, a comparable performance to the gold codes is achieved (Chapter 6). However, it is a challenging task to expand the code matrix further to accommodate higher number of cells. This is due to the fact that when truncating the Hadamard-Walsh matrix, the codes will be no longer Walsh codes and they will lose their properties.

4.4.3 Zero Cross-Correlation Complementary (ZCC) Sequences

Another group of codes has been investigated which originally used in radar systems are derived from complementary waveforms [23], [24]. Complementary waveforms are coded sequences with auto correlation that sums to zero everywhere except at match point. In addition to good auto-correlation, the waveforms used to generate the code tree here has minimum cross-correlation properties. Briefly, some of ZCC complementary codes main properties are summarized as follows:

- The rows of the code matrix represent ZCC codes.
- If the code is ZCC and complementary, then it is also a zero sidelobe periodic code (ZSPC), see [23].

The ZCC complementary code can be generated by the following equation [23]:

$$c_{mi} = \lambda^m d_{i+1} W_N^{M' mi} \quad m, i = 0, 1, \dots, N-1 \quad (4.9)$$

where W_N is defined as $W_N = e^{j\frac{2\pi}{N}}$, $\lambda \in \{1, W_N, W_N^2, \dots, W_N^{N-1}\}$, d_1, d_2, \dots, d_{N-1} are selected as random complex numbers and M' should be an integer which is prime to N .

Despite the fact that ZCC complementary codes will improve the positioning accuracy, it still very complicated to implement such sequences in practice since it can't be mapped to a conventional modulation scheme such as BPSK or QPSK (used in NB-IoT). Constellation diagram of ZCC code is shown in figure 4.16.

4.4.4 Barker Sequence Matrix

Barker sequence is a finite length binary sequence that consists of +1, -1 values with ideal auto correlation property. Only 8 known Barker sequences exist with its length vary from 2 to 13 [25].

In order to use Barker sequence for NB-IoT positioning purposes, we choose a Barker code of length 13 which has the following form: + + + + + - - + + - + - + (where + stands for +1 and - stands for -1). The choice of this length is decided since we need 12 values per cell ID. Based on this motivation, we omit the last digit (+1), after that, we build a code from Barker sequence consisting of real and imaginary part as follow:

$$C1 = [+1, +1, +1, +1, +1, -1, -1, +1, +1, -1, +1, -1] + j[+1, +1, +1, +1, +1, -1, -1, +1, +1, -1, +1, -1] \quad (4.10)$$

Next, we build a Barker Matrix (12×12) by circularly shift the Barker sequence, to guarantee that we have 12 codes with ideal auto-correlation properties as shown in Fig.4.17 supporting 12 different cell IDs.

However, Barker matrix codes still have very poor cross correlation due to the fact that each code is a circular shift of the original code. In order to improve the cross correlation, we multiply

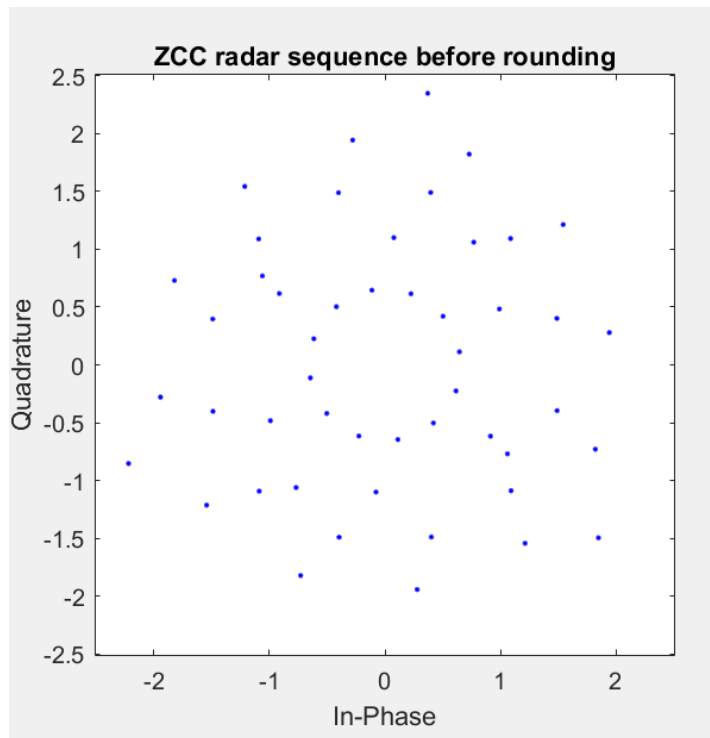


Figure 4.16: ZCC Sequence Constellation Diagram

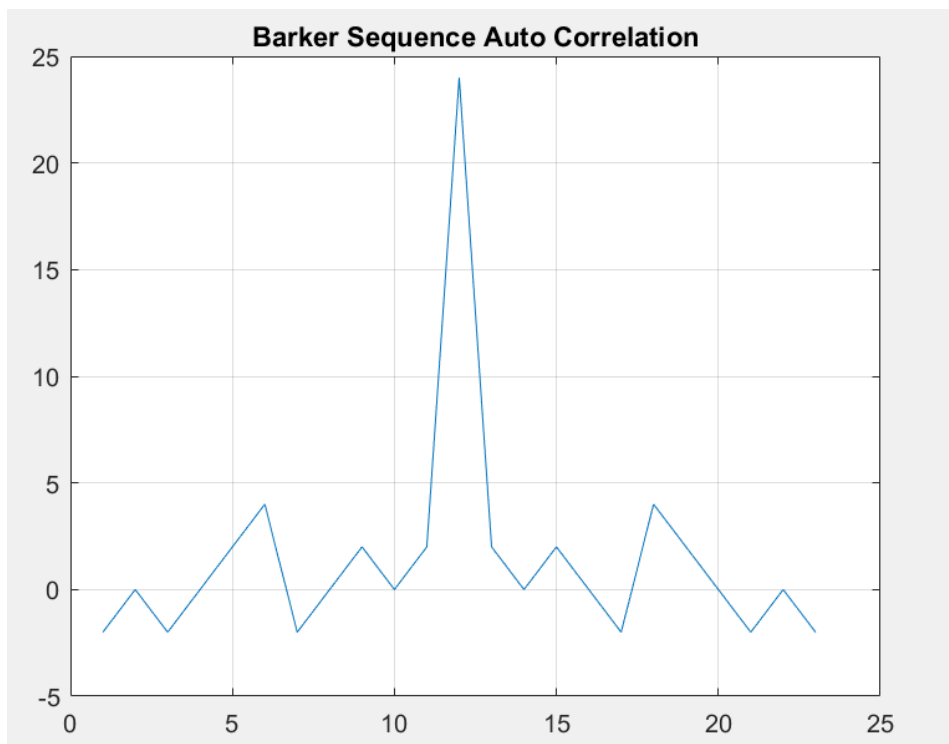


Figure 4.17: The Autocorrelation of Barker Sequence

Barker code matrix with W matrix defined as below:

$$W = W_N^{Mmj} \quad (4.11)$$

where in our thesis work, N is chosen to be 12, $M = 5$ and the parameters m and j range from 0 to $N-1$. Besides, W_N is defined as $W_N = e^{j\frac{2\pi}{N}}$.

The next challenge, is how to expand such matrix while keeping the good correlation properties in order to accommodate more cell IDs configurations. Several methods have been implemented and at the end, the decision was to generate different W matrices with different M values such as ($M = 1, 5, 7, 11$, etc), and multiply it with Barker matrix. Afterwards, we concatenate the final matrices together, mapping the values to conventional QPSK symbols and ending up with a big matrix accommodating $12 \times N$ codes, which can accommodate N cells. Finally, the codes are allocated to different cells and tested for positioning accuracy.

Drawbacks of such implementation are listed as follows:

- Performance Inconsistency. (since mapping the generated symbols to QPSK might end up leading to some codes with poor cross correlation properties), which leads to performance comparable or inferior to Gold Codes in some cases.
- Different cross correlation properties between different generated codes.
- Mapping the codes to known modulation schemes such as QPSK might lead to loss in accuracy but such loss is inevitable since the original codes are challenging to be implemented in hardware.

4.5 Expansion of PRS transmission in Time and/or Frequency

This section is dedicated to explain the process of either sending multiple subframes (in time) or multiple PRBs (in frequency). In NB-IoT applications where only a single PRB is supported in frequency domain, sending multiple subframes is a necessity to improve the positioning accuracy. While for MTC and LTE where more bandwidth resources are available therefore sending multiple PRB's is possible besides subframes which leads to further positioning enhancements. Sending multiple subframes should usually be accompanied with signal combiners at receiver side (more details in chapter 5 related to combination algorithms will be introduced). The more subframes sent, the better the accuracy achieved. Due to the fact that such method will improve signal quality reception and thus it leads to peak detection improvement mainly for cell edge UEs under different channel types (Additive White Gaussian Noise (AWGN), Extended Pedestrian A (EPA) and Extended Typical Urban (ETU)). The procedure is presented in Fig.4.18.

Lastly, to investigate how well positioning accuracy can be improved beyond NB-IoT, multiple PRBs are sent within a single subframe which leads to clear improvement in accuracy. Such method will greatly enhance the results, since the main lobe of the autocorrelation will become

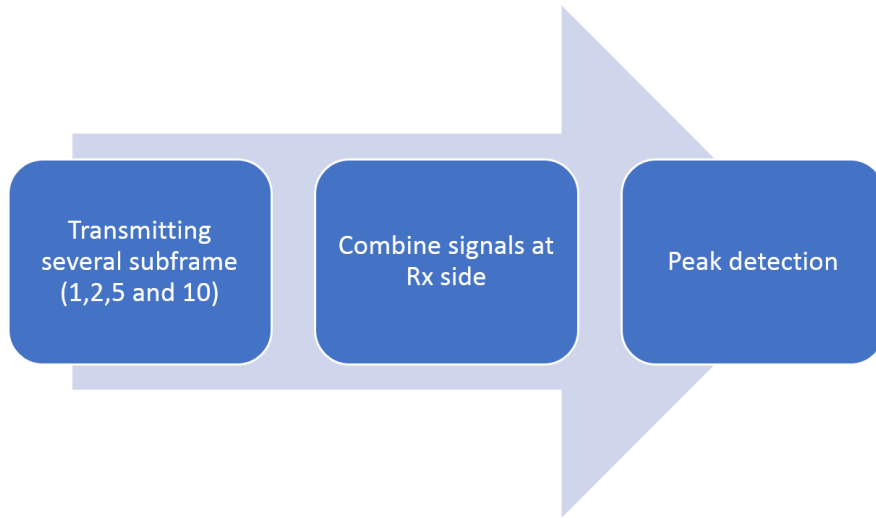


Figure 4.18: Multiple Subframe Transmission Procedure

narrower and subsequently improve peak detection at the receiver side. Auto-correlation of sending 1 subframe with either 2 consecutive PRB's or 4 consecutive PRB's is as shown in Fig.4.19.

In order to further enhance positioning, sending multiple subframes configured with multiple PRBs is followed in systems beyond NB-IoT.

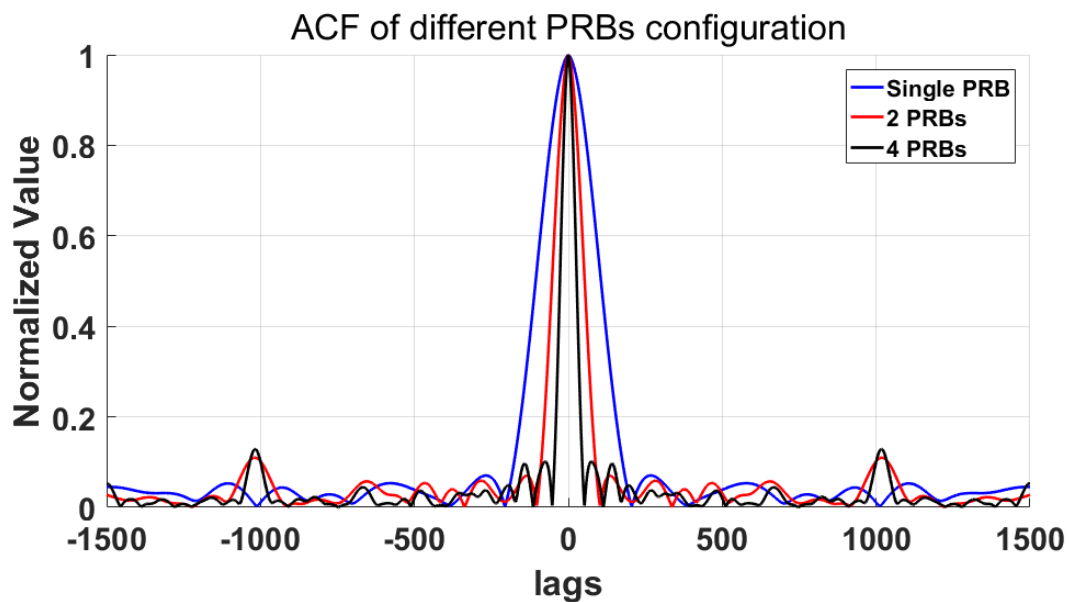


Figure 4.19: ACF of Gold sequence with different PRBs Configuration

RECEIVER DESIGN

Chapter 5 tackles the structure of NB-IoT receiver used for positioning purposes. Under the framework of this thesis work for OTDOA positioning, the receiver operates as a correlator to estimate the position. Basically by finding the estimated TOA based on the correlation results between the transmitted reference signal of each eNB and the received signals.

In this chapter, the first section introduces various channel models based on 3GPP TS 36.104 [26]. Section 5.2 briefly presents the general receiver block diagram. After that, section 5.3 mainly covers different combination algorithms, provided that multiple subframes are sent at the transmitter. Then in the following Section 5.4, different correlator designs are illustrated. Finally in the last Section 5.5, interpolation and estimator principles and their influences on positioning accuracy explained.

5.1 Channel models

In this section, we will briefly illustrate different channel models investigated in our thesis work. In the first step, two frequency flat channel models will be introduced and investigated. Secondly, two typical 3GPP frequency selective fading channel models are presented. To overcome the channel fading, simple equalization approach is going to be introduced in the combiner section 5.3, keeping in mind that more advanced channel estimation and algorithms are beyond the scope of this thesis work.

5.1.1 Frequency Flat Fading Channel Model

According to [27], frequency flat fading channel model follows the assumption that the bandwidth of transmitted signal is much narrower compared with the coherent bandwidth of the wireless

propagation channel. Therefore, the channel attenuations are equivalent throughout the whole frequency band occupied by the transmitted signal. Such channel model leads to the fact that propagation channel can be simplified as a complex number instead of a transfer function. The complex number represents both the attenuation and phase rotation during signal propagation across the channel.

In this thesis work, the propagation channel model is initially assumed as a large-scale fading channel with the presence of Additive White Gaussian Noise (AWGN). The reason behind our assumption is to effectively compare the performances of different transmitted sequences. In the second step, we consider the effect of a type of small-scale fading (frequency flat fading) to our propagation channel. The block diagrams of these two channels are presented in Figs.5.1 and 5.2.

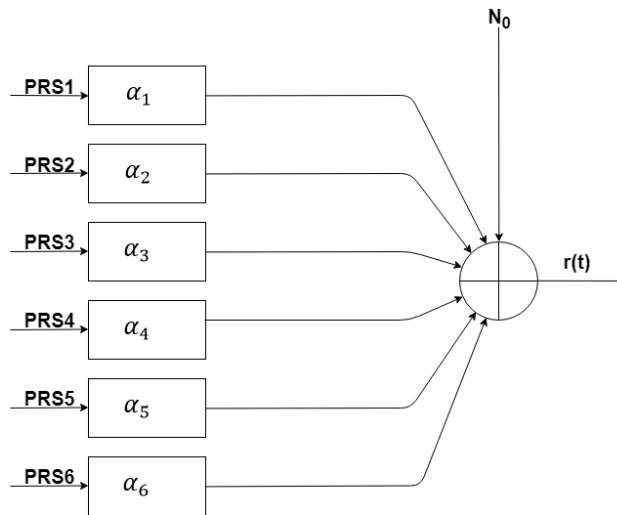


Figure 5.1: Basic Large Scale Fading Channel

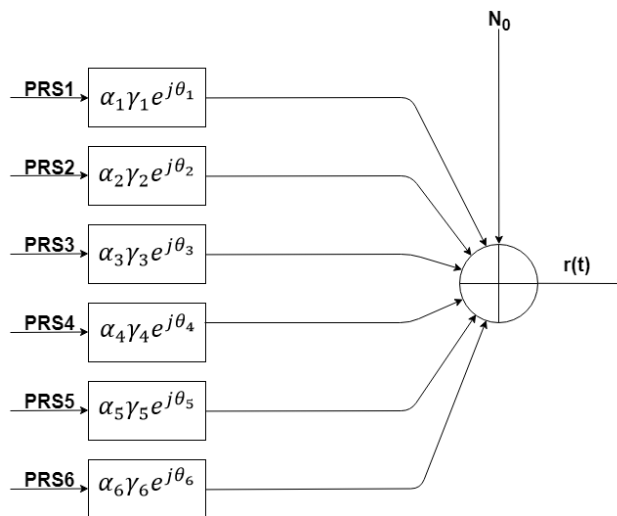


Figure 5.2: Frequency Flat Fading Channel

As shown by Fig.5.1, six positioning reference signals are transmitted at the same time by corresponding eNBs. It is worthwhile to notice that since the distances between each eNB and the UE are different. Therefore, the attenuations during the propagation, which represented by α_i , also differ from each other. Based on our basic large-scale fading model, α is denoted as the shadow fading parameter and therefore the value of which should be a real number that does not include phase rotation. At the receiver side, the user equipment receives the sum of all attenuated noisy signals transmitted by 6 eNBs. It is worth mentioning that we define the signal to noise ratio (SNR) of our system as the ratio of the power of the received signal transmitted by the serving eNB and the power of the noise.

In our second assumption, an insight of small-scale fading is introduced to our system by multiplying a complex number as shown by Fig.5.2, it is noticed that $\gamma e^{j\theta}$ is added onto the large-scale fading parameter α . The parameter γ is denoted as the amplitude variation while θ represents the phase rotation of signals during channel propagation.

5.1.2 Frequency Selective Fading Channel Model

Provided that the bandwidth of the transmitted signal is much wider than the coherent bandwidth of the propagation channel, then the fading of different frequency components within one transmitted signal will be uncorrelated. Therefore, we can characterize the property of this specific channel via transfer function or the Inverse Fourier Transform of it, in what so-called, impulse response. Compared with the transfer function representation, the impulse response directly indicates the numbers and attenuations of each channel tap. Thus this representation is utilized as the definition of various kinds of frequency selective fading channel in the 3GPP TS 36.104 Annex B [26]. In our thesis work, two types of frequency-selective fading channel models are investigated, namely Extended Pedestrian A (EPA) and Extended Typical Urban Channel (ETU). Channel delay profiles of EPA and ETU illustrated by tables 5.1 and 5.2, according to the definitions stated by 3GPP.

As indicated in Tables 5.1 and 5.2, the duration of EPA multipath channel impulse response

Table 5.1: PDP of EPA Channel Model

Excess tap delays [ns]	Relative power [dB]
0	0
30	-1
70	-2
90	-3
110	-8
190	-17.2
410	-20.8

Table 5.2: PDP of ETU Channel Model

Excess tap delays [ns]	Relative power [dB]
0	-1
50	-1
120	-1
200	0
230	0
500	0
1600	-3
2300	-5
5000	-7

of EPA is 410 ns, and consists of 7 delay profile taps. The first tap has the maximum energy distribution that can refer to Line of Sight (LOS) component. While for the following taps, it is noted that with increasing tap indication, energy distribution becomes less. On the other hand, for ETU channel, impulse response length corresponds to 5000 ns where the 3rd, 4th and 5th taps have the highest power as 0 dB, while overshadowing the LOS, 1st and 2nd taps by 1 dB.

5.2 Receiver Structure

Compared with the ordinary detectors implemented to recover the original data, the approach of OTDOA positioning receiver is to estimate the position of the target UE by computing TDOA of multiple positioning reference signals. Thus, the receiver for positioning acts as a correlator as can be seen in the block diagram given by Fig.5.3.

As depicted in Fig.5.3, the receiver utilized for positioning consists of 5 main parts. Firstly, the signal is demodulated so that interference from other frequency bands will be removed. After the demodulation procedure, channel identification will be conducted so that the receiver can achieve the estimation of the channel impulse response. In our thesis work, we assume that the first two steps have already been implemented by other blocks included in the receiver chain. After estimating the channel properly, received signals are fed to the combiner where different copies of the signals are combined by means of two different methods, either incoherent or coherent combining. Afterwards, the correlator will compute the correlation between the received signal and the transmitted pilots. Finally, the peak detector aims at finding the first peak of the correlation result such that the time of arrivals can be estimated.

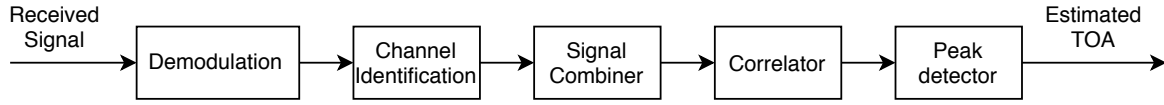


Figure 5.3: Receiver Structure

5.3 Combiner Design

When multiple subframes are transmitted by eNBs, it is of necessity to combine the received signal effectively so that the diversity can be achieved in time domain. Two main types of combiners have been considered, namely incoherent and coherent combiners. The former combiner processes the signal by calculating the average of multiple subframes signals which will lead to noise power reduction while the latter combiner is able to leverage the aid of different combination schemes such as Zero Forcing (ZF), Minimum-mean Square Estimation (MMSE) and Matched Filter (MF). Additionally, it is of high importance to emphasize that channel estimation has been previously implemented and perfect channel knowledge at receiver is assumed.

5.3.1 Incoherent combiner

As previously mentioned, the main objective of this receiver is to average the received signals via multiple subframes. Its process can be explained as follow: supposing that a total number of N subframes are transmitted by the transmitter, the receiver can therefore collect N copies of signals. Here, we denote the received signal as $y_i(n), i = 1, 2, \dots, N$ and the combined signal as $z(n)$ where n stands for discrete time symbols. Such that the combined signal can be written as

$$z(n) = \frac{1}{N} \sum_{i=1}^N y_i(n) \quad (5.1)$$

5.3.2 Coherent combiner

Coherent combiner can effectively use channel knowledge acquired by the receiver to significantly improve the positioning accuracy. At first, a simple approach channel estimation will be illustrated (keeping in mind that it is only done for study purposes since real channel equalization has been already conducted in real situations under the operation of different blocks). Later on, the analysis and comparison of three combination schemes, namely, ZF, MMSE, MF will be presented.

5.3.2.1 Channel preprocessing

By reviewing the definitions of EPA and ETU channel proposed by the 3GPP standard, we notice that the maximum time delays of taps for EPA and ETU channel are shown as 410ns, and 5000ns, respectively. On the other hand, the sampling rate of the NB-IoT receiver is downsampled as 1.92 MHz according to the standard, in order to both simplify the complexity of hardware design and reduce the energy consumption.

By simple calculation, it can be shown that the sampling period of NB-IoT receiver is approximately 520ns, therefore it is reasonable to sum values of all taps of the EPA impulse response together and consider the channel response as a complex number. For ETU channels, the same approach can be applied since the total length of all 9 delay taps turns out to be close to the duration of 10 samples. However, the cyclic prefix of our NB-IoT OFDM symbol is 9 samples, which means only one sample difference compared with the total length of multipath delays. Additionally, by referring to Table 5.2, the last tap has 7 dB difference compared with the strongest path.

5.3.2.2 Channel matrix for multiple subframes transmission

We hereby process the channel knowledge by approaches mentioned in the previous sub-section. However, in this section since the positioning signals are assumed to be transmitted by multiple copies over several subframes, it is more accurate to characterize the propagation channel as a matrix H , which is given by:

$$H = \begin{bmatrix} h_{11} & \dots & h_{61} \\ \vdots & \ddots & \vdots \\ h_{1N} & \dots & h_{6N} \end{bmatrix}$$

Each column of the H matrix represents the channel between one UE and all 6 eNBs at a certain subframe, while each row of the Matrix indicates the channel response of different subframes corresponding to a specific eNB. Additionally, we denote the transmit vector as x , the noise vector as n , the received vector as y , thus the received vector can be shown as:

$$y = Hx + n \quad (5.2)$$

5.3.2.3 Coherent combination schemes

Received signals coherent combining helps to improve positioning accuracy to a large extent in comparison to incoherent combination scheme. Three coherent combination schemes (ZF, MMSE, MF) are tested by this thesis simulation platform. In this section, a brief introduction and comparison of these schemes will be provided [28] while the simulation results will be shown in Chapter 6. We denote matrix G as the processing matrix, z as combiner output, y as the received signal apparently:

$$z = Gy \quad (5.3)$$

(1) Zero Forcing (ZF)

The mathematical expression of zero forcing matrix is given by,

$$G = H^+ \quad (5.4)$$

where H^+ is defined as the pseudo inverse for the channel matrix H , specifically:

$$H^+ = (H^H H)^{-1} H^H \quad (5.5)$$

(2) Minimum mean square error (MMSE)

As to MMSE combining scheme, the processing matrix is shown as,

$$G = H^H (H R_{xx} H^H + N_0)^{-1} \quad (5.6)$$

Where R_{xx} stands for the correlation matrix of the transmitted signal, and N_0 represents the noise power spectral density.

(3) Matched Filter (MF)

The definition of the processing matrix of MF combining is denoted as,

$$G = H^H \quad (5.7)$$

which is the conjugate transpose of the channel matrix H .

Making Comparison of these three kinds of combiners, ZF is designed to completely remove the interference of signals from other eNB. If the system operates in a high SNR situation, this combination scheme can effectively separate the signals from all eNBs. However, the drawback of ZF combiner is that it might lead to noise enhancement, deteriorating the combination performance. Secondly, Applying matched filter operation to the receiver can help to alleviate the hardware complexity besides maximizing the signal to noise ratio. However, the interference of signals from other transmitters may turn out to be stronger compared with other two schemes. Lastly, the main principle of MMSE operation is to minimize the mean square error between transmitted and received signals, thus it can achieve a good tradeoff between suppressing noise and reducing the interference. Nevertheless, the calculation complexity increases and it is necessary to measure the SNR at the receiver side [28].

5.4 Correlator design

For OTDOA positioning scheme, the correlator plays an important role at the receiver side, since it helps to compute the correlation between the received signal and the transmitted pilots. Correlation output acts as an input to the peak detector, such that the time delays of signals' initial paths transmitted by eNBs can be estimated. Following the assumption that the transmitted symbols act as reference symbols at receiver side during the correlation process. Two types of correlators are investigated and implemented during this thesis work, namely, time domain and frequency domain correlators.

5.4.1 Time domain correlator

The time-domain correlator processes the TOA estimation assignment by calculating the cross-correlation function between the received signal and the transmitted pilot in time domain.

Reviewing the design of the time-frequency resource grid, 8 symbols out of 14 are occupied by positioning reference signals, provided that the NB-IoT positioning system operates in in-band mode. During this thesis work, the correlator is designed to process the resource grid symbol by symbol, which calculates the cross-correlations between the received signal and the pilots transmitted by each e-NodeB for each symbol. The mathematical expression of this cross-correlation is given by

$$R_{p,l}[n] = \frac{1}{M} \sum_{m=n}^{n+M-1} y(m+lM) s_{p,l}^*[m-n], n = 0, \dots, \tilde{M} \quad (5.8)$$

Where $R_{p,l}$ stands for correlation output, y corresponds to received signal, s represents the reference symbol, M and \tilde{M} stand for the overall number of symbols and the maximum delay respectively.

After collecting all eight cross correlation outputs, the average of all is computed and the result will be fed into the peak detector. The OTOA of each eNB can be achieved by finding the delay corresponding to the peak of the correlation. Further details related to peak detector design and operation will be explained in the next section.

5.4.2 Frequency domain correlator

In order to accelerate the processing speed and reduce the computation complexity, a different design of correlator has been implemented in frequency domain. Mathematically, the result of the frequency domain correlator provides the same result as the time domain one, since the correlation operation in time domain corresponds to the multiplication in frequency domain. However, leveraging the IFFT and FFT operation, the complexity of calculation will be effectively simplified so that the power consumption can get significantly improved as can be seen in Sub-section 5.4.3.

Here, the received signal is denoted as $y(n)$, and the reference signal as $s(n)$. Then after the Fourier transform, the frequency spectrum of both signals are presented as:

$$Y(k) = \sum_{n=0}^{N-1} y(n) e^{-j \frac{2\pi kn}{N}} \quad (5.9)$$

$$S(k) = \sum_{n=0}^{N-1} s(n) e^{-j \frac{2\pi kn}{N}} \quad (5.10)$$

Afterwards, IFFT is applied to $Z(k) = Y(k) \times S(k)^*$, according to [29], the circular correlation of $y(n)$ and $s(n)$ can be generated by $Z(n)$, where

$$z(n) = \frac{1}{N} \sum_{k=0}^{N-1} Z(k) e^{+j \frac{2\pi kn}{N}}. \quad (5.11)$$

Structure of the frequency domain correlator can be seen in Fig.5.4. As depicted in Fig.5.4, both the received signal and the reference signal are input to the correlator at the first stage. In

the next step, we transfer both into frequency domain by the aid of Fast Fourier Transform (FFT). Afterwards, the received signal is multiplied by the conjugate of the reference signal, followed by the IFFT operation, transferring the signal back to the time domain. Finally, a peak detector collects the output of the IFFT and computes the delay, labeled as the estimated TOA.

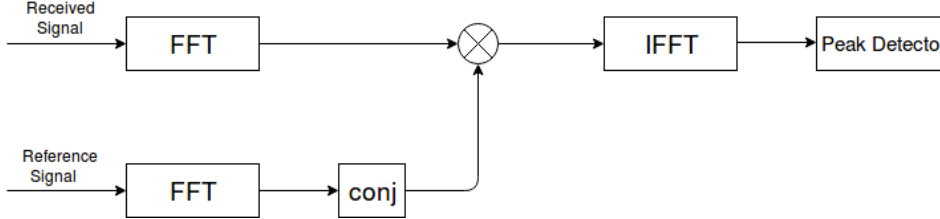


Figure 5.4: Frequency Correlator

The main benefit of applying the frequency correlator is to reduce the calculation complexity by the aid of FFT. According to [30], applying FFT operation returns exactly the same result as DFT, but the computation complexity has been reduced to such an extent that it is affordable for ordinary home computers. Moreover, FFT holds all the properties as well as drawbacks of DFT, such as linearity, symmetry, leakage, etc.

Based on our receiver implementation, the correlator processes the received signal symbol by symbol. According to the LTE standard, the FFT size of each transmitted symbol is 2048 and the receiver downsamples the size to 128 by a factor of 16. In addition, considering the CP added to the symbol and the delay caused by the propagation, the overall length of the received signal for each symbol exceeds 128. Therefore, the FFT size of the receiver is set as 256 since the FFT size is normally selected as an integral power of 2, see [30].

5.4.3 Computation Complexity Analysis

Owing to the efficiency of FFT in terms of computation complexity simplification, convolution and correlation calculations are often conducted by FFT in frequency domain, see [30]. Here, the comparison between computation complexity of time and frequency domain correlators is explained below and clarified in the following table

Table 5.3: Computation Complexity Analysis

Number of Points	Complex Multiplications of DFT	Complex Multiplications of FFT
N	N^2	$N/2 \log_2 N$
256	65536	1024

Supposing that the FFT method is selected to be “radix 2-FFT” and the FFT size is denoted as N , the complex multiplication numbers needed is approximately $N/2 \log_2 N$. According to the block diagram illustrated in Fig.5.4, in total the numbers of FFT/IFFT operations are shown as

three and the FFT size is chosen as 256. Therefore, the overall complex multiplications needed for the frequency domain correlator are 3072. Compared with the time domain correlator where the complex multiplication numbers D^2 are needed, D stands for signal length which includes transmitted symbols, CP, and delays. It is apparent that the computation complexity can be significantly reduced by frequency domain correlator.

5.5 Peak Detector

5.5.1 Introduction

As the last block in the receiver chain, the peak detector provides estimation for the delays $n_{p,0}$ of the initial path related to the signal transmitted by each eNB. Taking the correlation function between the received signal and the transmit pilot as input, the peak detector generates 6 TOAs corresponding to each eNB. Under the assumption of AWGN channel, the maximum likelihood estimation of the delay for eNB number p can be expressed as, see [31]:

$$\hat{n}_{p,0} = \arg \max_n \left| \sum_{s=0}^{N_{NPRS}} R_{p,\tilde{l}(s)}[n] \right| \quad (5.12)$$

Where N_{NPRS} represents the total numbers of NPRSs in a single subframe, the function $R(n)$ indicates the cross-correlation defined in Section 5.4, the function $\tilde{l}(s)$ denotes the s th symbol in one resource grid used by NPRS.

According to 5.12, the main goal of the peak detector is to detect the index n , which maximizes the absolute value of the sum of the correlation over all symbols containing NPRS. After achieving the time delay samples $\hat{n}_{p,0}$ for each eNB, the TOA estimated in the unit of seconds can be calculated by

$$\hat{\tau}_{p,0} = \frac{\hat{n}_{p,0}}{F_s} \quad (5.13)$$

Where F_s represents the sampling frequency used by the NB-IoT receiver. Apparently, the choice of sampling rate determines the minimum resolution of TOA. Since the NB-IoT receiver reduces the sampling rate, a relatively low resolution will affect the accuracy of positioning. In order to compensate for this problem, interpolation techniques can be applied to correlation results which will be illustrated shortly.

In order to remove the false peak in the correlation, it is of necessity to calculate the peak to average ratio (PAR) and make comparison between this value and present threshold γ . The definition of the PAR is expressed as, see [3]:

$$PAR = \frac{|\sum_{s=0}^{N_{NPRS}-1} R_{p,\tilde{l}(s)}[\hat{n}_{p,0}]|}{\frac{1}{\tilde{M}} \sum_{n=0}^{\tilde{M}} |\sum_{s=0}^{N_{NPRS}-1} R_{p,\tilde{l}(s)}[n]|} \quad (5.14)$$

Where \tilde{M} stands for the maximum delay. Not all measurements can be considered for peak detection, since some of PAR values are smaller than the defined threshold, which in turn means

that those peaks are not qualified. Therefore, such measurements will be discarded. Hence, a decent selection of this threshold γ can balance the probability rate of false alarm and miss detection.

5.5.2 Resolution Enhancement by Correlation Interpolation

NB-IoT reduces the sampling rate for the sake of lowering down the power consumption, that leads to a lower resolution of TOA and deteriorates the positioning accuracy. However, interpolating the cross-correlation function can help to compensate the resolution loss and enhance the positioning performance [3]. Here, we denote V as the interpolation factor and W the size of window around the preliminary estimated TOA \tilde{n}_p , the correlation function after interpolation can be illustrated as:

$$\hat{R}_p[n] = \sum_{m=\tilde{n}_p-W}^{\tilde{n}_p+W} R_p[m] \frac{\sin \pi(\frac{n}{V}) - m}{\pi(\frac{n}{V}) - m}, n = -VW, \dots, VW \quad (5.15)$$

As shown in the equation, if the interpolation factor is selected as 16, the sampling rate will be elevated from 1.92MHz to 30.72 MHz. The enhancement of positioning accuracy can be achieved provided that the system SINR value is fair enough, because it is important to ensure that the positioning signal rather than noise is interpolated.

5.5.3 The Position Estimation Solutions

A. Elimination of Unqualified TOA

Due to the presence of channel fading and noise, it is challenging for the peak detector to always give perfect TOA estimation. Apparently, unrealistic estimation will deteriorate the positioning performance, thus it is indispensable to discard the unqualified TOA. Check Fig.5.7 which clearly shows the improvement of such estimation approach.

Our approach is to improve estimator operation by setting an upper bound that is defined as follow:

- Maximum distance is set to be around 3.6 km (which is almost twice the inter site distance configured as 1732m)
- Associated maximum TOA is calculated and it turns out to be equal to around 12e-6 seconds (3.6km/speed of light)
- Any TOA with value larger than this upper bound will be discarded and not considered in the calculation.

The above operations are illustrated in Figs.5.5, 5.6 and 5.7.

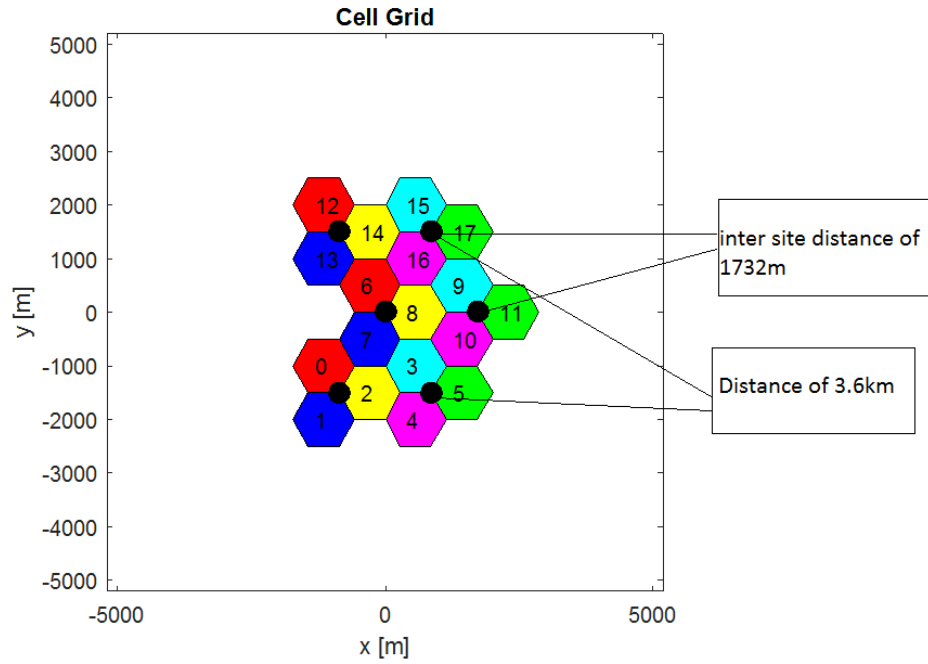


Figure 5.5: eNB's Map [3]

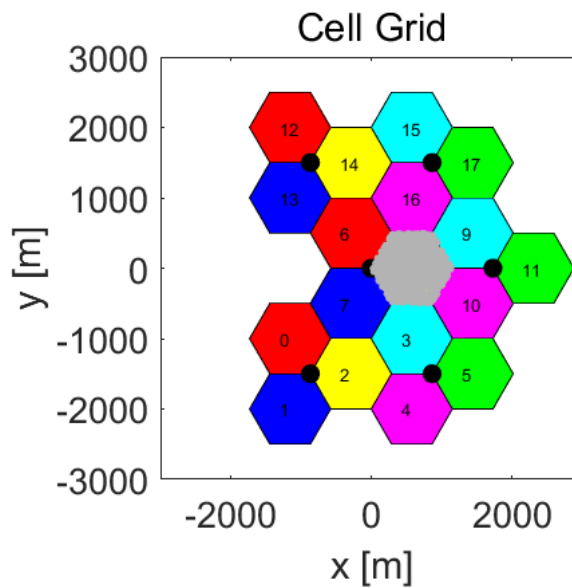


Figure 5.6: UEs dropped under certain cell

B. The positioning calculation

The position of a UE cannot be directly computed by TOAs achieved by the peak detector, since the receiver lacks the knowledge of signal transmission times. Therefore, it is necessary to assign an eNB as the reference cell, say eNB 0, and the TOA of this eNB is expressed as $\tau_{0,0}$. Once achieving the TOA estimation of other eNBs, the TDOA between the reference eNB and other

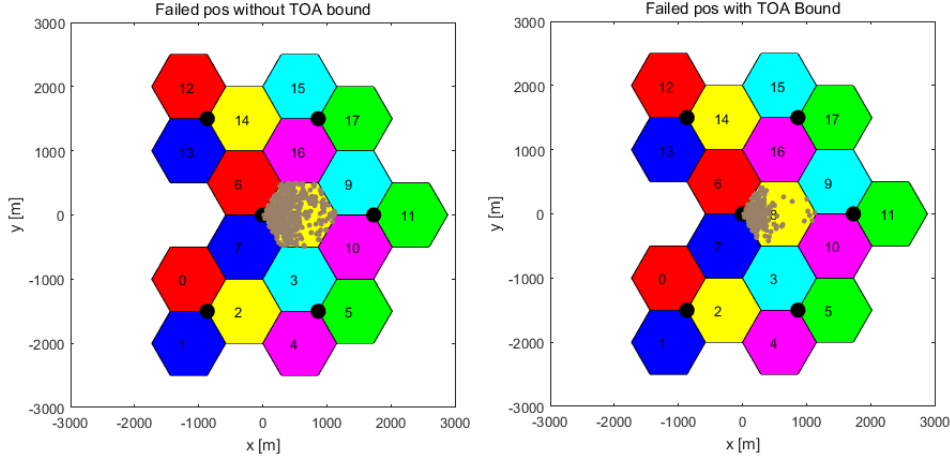


Figure 5.7: Less dropped UE with better Estimator

eNBs can be computed, such as:

$$\Delta \hat{t}_p = \hat{t}_{p,0} - \hat{t}_{0,0}, \quad p = 1, \dots, P-1 \quad (5.16)$$

Afterwards, estimated TDOAs will be transmitted back to the base station, followed by computing the position of the UE by finding the solutions of the equations expressed below:

$$\begin{cases} c\Delta \hat{t}_1 = \sqrt{(x-x_1)^2 + (y-y_1)^2} - \sqrt{(x-x_0)^2 + (y-y_0)^2} \\ c\Delta \hat{t}_2 = \sqrt{(x-x_2)^2 + (y-y_2)^2} - \sqrt{(x-x_0)^2 + (y-y_0)^2} \\ \vdots \\ c\Delta \hat{t}_{P-1} = \sqrt{(x-x_{P-1})^2 + (y-y_{P-1})^2} - \sqrt{(x-x_0)^2 + (y-y_0)^2} \end{cases} \quad (5.17)$$

In this equation, the positions of eNBs are provided and it is assumed that these positions are accurate enough. Moreover, each equation in the group generates a hyperbola and UE position can be achieved by solving the intersection points of these hyperbolas. Thus, at least three qualified TOAs are required ($P = 3$), otherwise there may exist several intersection points satisfying the equation. Supposing that the numbers of qualified TOA are greater than 3, then least square estimation method can be applied to estimate the UE position.

SIMULATION RESULTS

In this chapter, simulation results of OTDOA positioning using Monte Carlo method will be presented and the platform of which has been built using MATLAB. Initially, Graphical User Interface will pop out where several parameters can be configured (such as number of eNBs, number of UEs, SNR value, etc). Alongside different simulation schemes can also be selected, details of choices are presented in Fig.6.1.

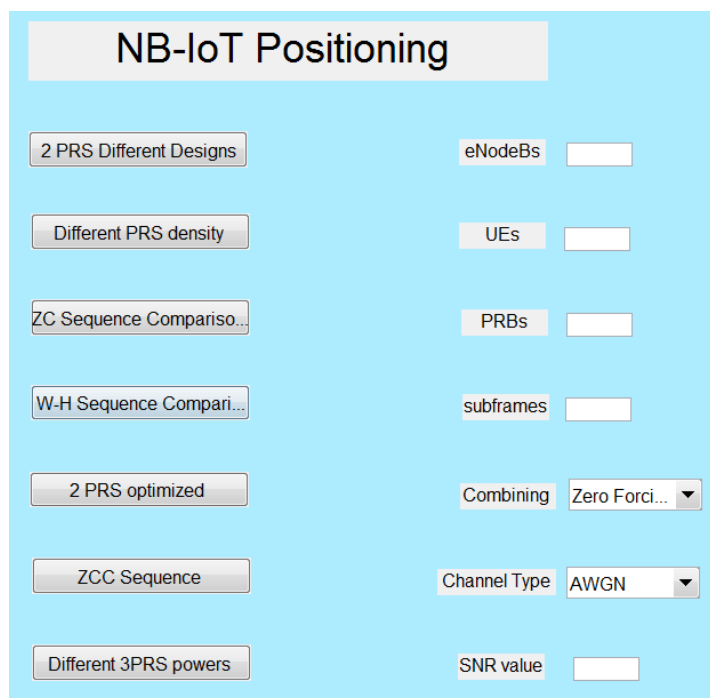


Figure 6.1: GUI Screen

6.1 Simulation Assumptions

Firstly, hexagonal cell structure is created based on the input eNBs numbers (a maximum of 19 can be supported) with a certain inter-site distance according to [32], as illustrated in Fig.6.2. Afterwards, the input numbers of UEs will be dropped uniformly in a certain cell in order to effectively evaluate the positioning accuracy. As presented in Fig.4.1, the transmitted signal will be created based on the inputs (such as the sequence choice, numbers of subframes, etc). In the next stage, the transmitted signals will undergo different propagation channel effects that will be created based on the input settings (AWGN, EPA, etc.). Keeping in mind that each UE will experience a different large-scale fading due to the fact that the distance between each UE and eNB (6 in total) is different from one another. After that, the created unique received signals per UE will be processed by the receiver starting from combination scheme and ending with the interpolated estimated UE position errors, the receiver process has been covered in details in the previous chapter. Additionally, a map presents the failed UE estimations as depicted in Fig.6.3, which does not satisfy the evaluation criteria followed:

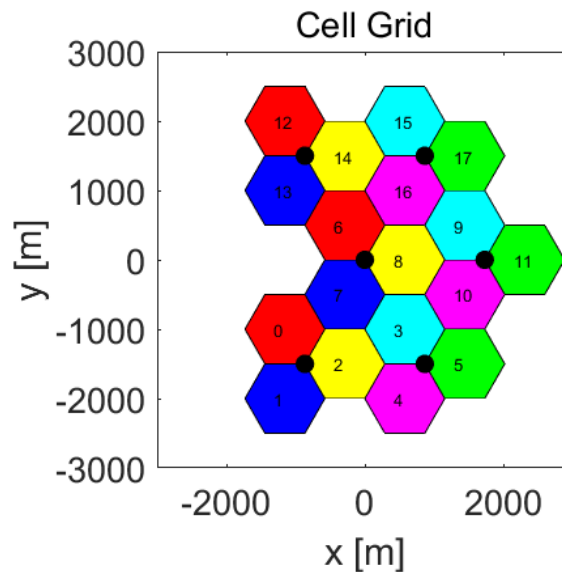


Figure 6.2: Sites Cell Grid

- Numbers of Failed Peak detections lead to insufficient TOA estimations to properly perform OTDOA (At least three cells are essential).
- The estimated position errors are more than 250m.

The positioning accuracies will be analyzed based on the CDF curve. At Section 6.1, different PRS densities will be analyzed, followed by the analysis of different 2PRS designs in Section 6.2. Afterwards, in Section 6.3, different sequences introduced in chapter 4 performance will be

studied. After that, in Sections 6.4 and 6.5, 2 PRS optimized sequence and multiple subframes as well as different combiner simulation test will be presented respectively. Thereafter, multiple PRBs performance will be illustrated in Section 6.6. Finally, in Sections 6.7 and 6.8, EPA channel then different SNR values performance results will be evaluated. The simulation parameters are illustrated by Table 6.1, if not specially emphasized.

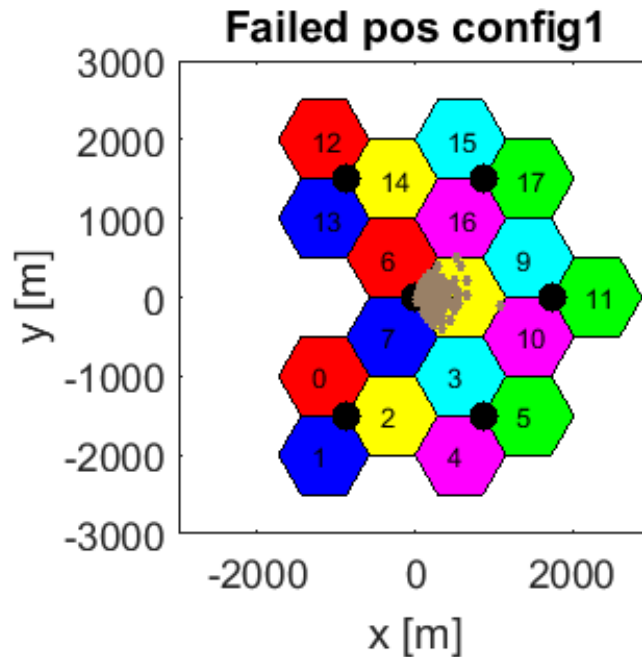


Figure 6.3: Failed Detected UEs

6.2 PRS density

The simulation results in terms of different PRS densities configuration within a single Resource Block are presented in Figs.6.4 and 6.5. As shown, the performance of 3 PRS density (where each eNB occupies 3 REs in a single OFDM symbol) overshadows the 2 PRS original by approximately 5 meters, provided that 4 eNBs operates in the system. However, due to transmitted signal collision in the frequency domain, the accuracy of 4 PRS signals is unsatisfied. While for 6 eNBs configuration (6 different Cell IDs), we clearly see that the performance of 3PRS per symbols deteriorates due to the fact that inter-cell interference increased, chances of RE collisions are higher and in case of RE collision occurrence, it will be challenging to mitigate it.

6.3 Different Time Frequency Resource Grid Design

In this section, the simulation results according to different time-frequency resource grid designs which introduced earlier in Chapter 4 Section 4.2 (from Figs.4.7 till 4.12) will be presented in

Table 6.1: Simulation Parameters Settings

Parameters	Values
Numbers of eNBs	as input parameter (default is 6)
Numbers of UEs	as input parameter (default is 1000)
Intersite-distance d	1732m
Operation Mode	In-band
Channel model	AWGN, EPA, ETU
Doppler Frequency Shift	3Hz(Configurable)
Consecutive NPRS Subframes	as input parameter
Consecutive PRBs	as input parameter
NPRS muting	NA
UE sampling frequency	1.92MHz
Standard Deviation for Shadowing	8dB
Inter-cell shadowing correlation	0.5
Pass Loss model(r_p in km)	$(\alpha_p)_{dB} = 120.9 + 37.6 \log_{10} r_p$
Interpolation factor	16
Interpolation window	8

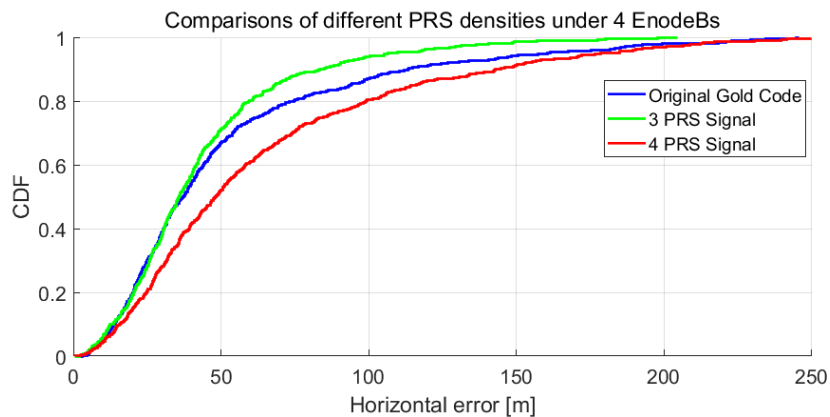


Figure 6.4: 4 eNBs performance

Fig.6.6. As can be seen comparable performance of all the designs can be noted under cell ID from (0 to 5) except for design 2 introduced earlier in Section 4.2.2 which shows a better accuracy by almost 9 meters. An important thing to highlight about the PRS with gold codes performance when processing only a single subframe is that its performance will be highly inconsistent and unpredictable according to which cell ID's included in OTDOA positioning process. Due to such issue, we cannot confirm that the performance of the second design will always be better than the original. In order to resolve such problem, it is recommended to transmit several subframes and combine them at receiver side.

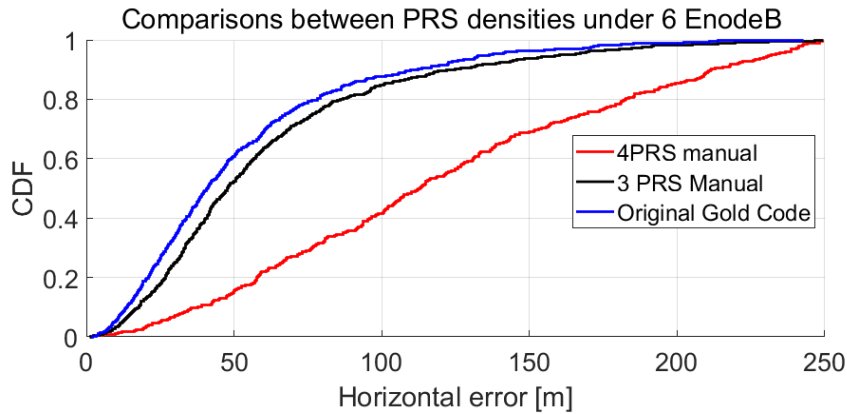


Figure 6.5: 6 eNBs performance

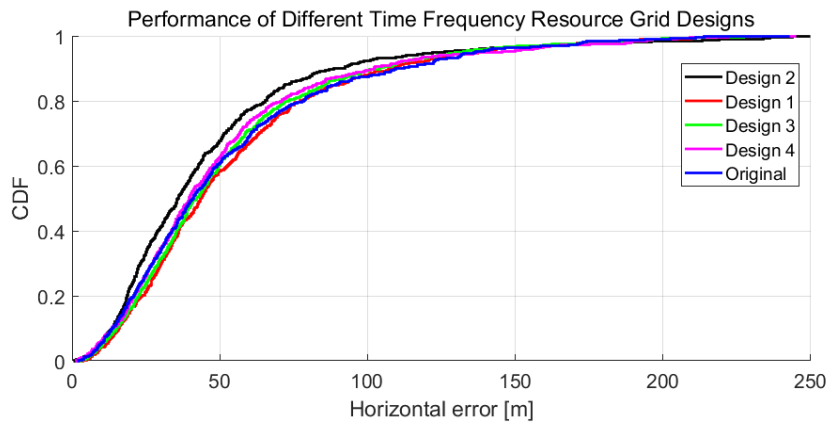


Figure 6.6: Different 2 PRS designs performance

6.4 Different Sequence Comparison

Performance comparison of different sequences will be presented by Figs.6.7 till 6.10 and analyzed in this section. The sequences to be covered are the ones introduced earlier in Chapter 4 which can be shortlisted as follows.

- Hadamard-Walsh Sequence
- ZC Sequence
- ZCC Sequence
- Barker Sequence

and the simulation is conducted for AWGN channel using 6 eNBs where Cell IDs ranging from 0 to 5 with only a single subframe sent and the accuracy evaluation is based on interpolated CDF value of 0.7.

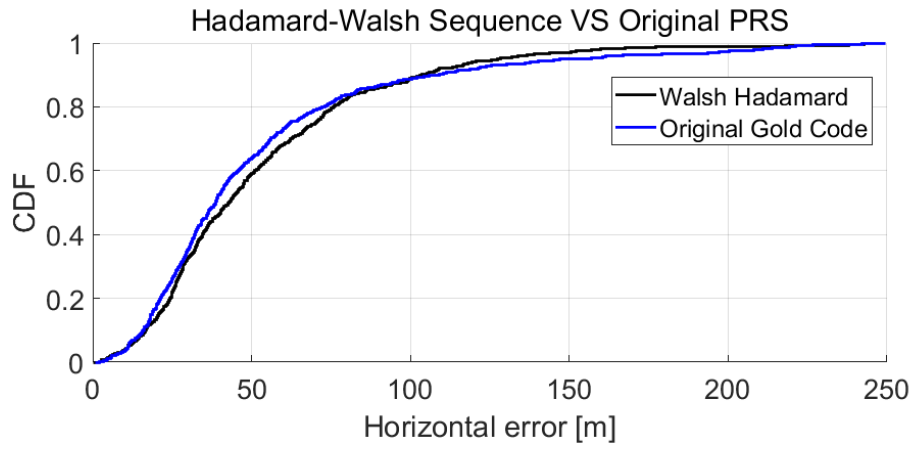


Figure 6.7: Positioning Accuracy of Walsh-Hadamard Sequence

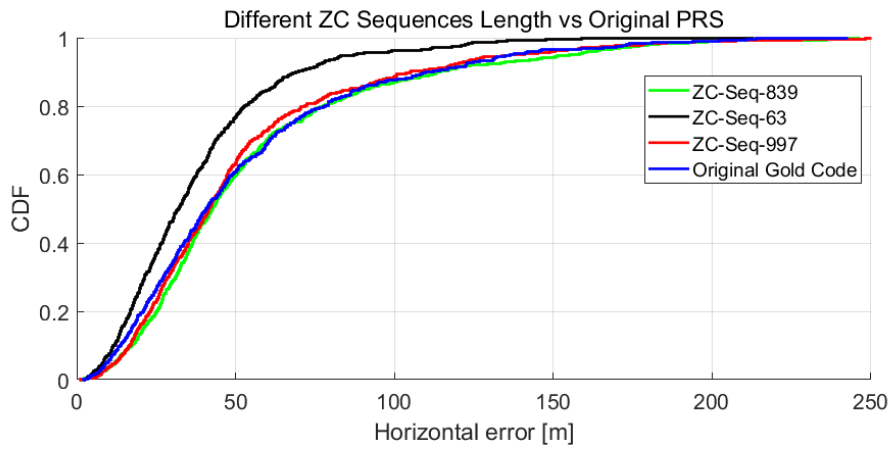


Figure 6.8: Comparisons of different ZC sequences with the Gold Sequence

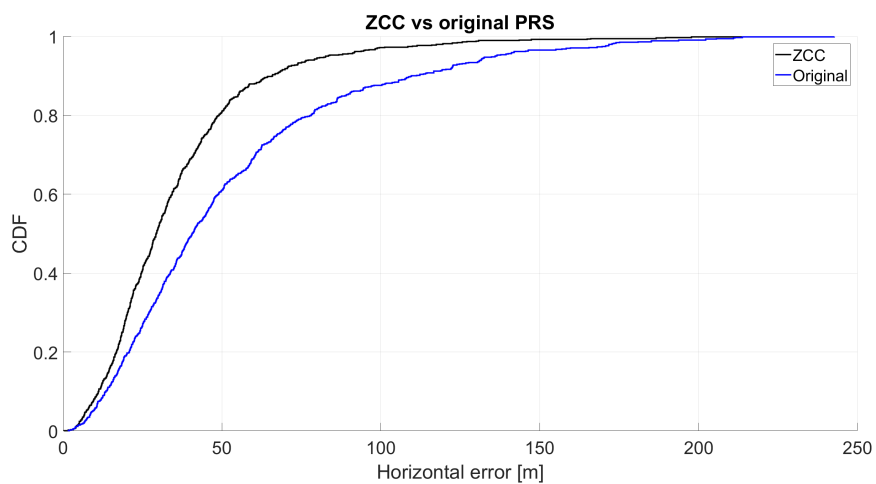


Figure 6.9: Comparisons of ZCC with the Gold Sequence

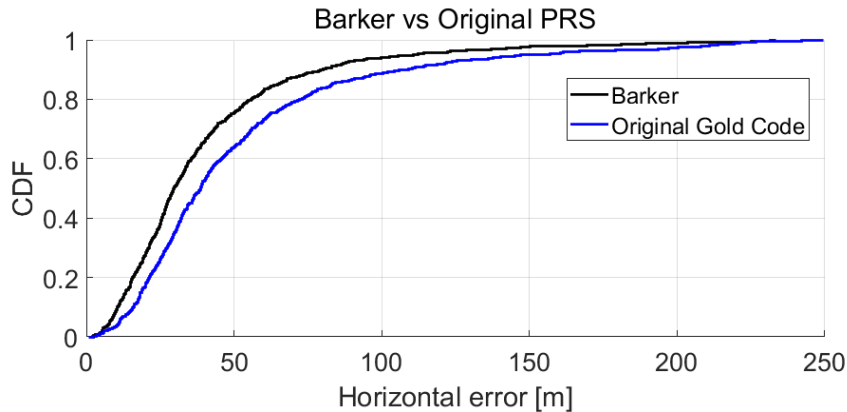


Figure 6.10: Comparisons of Barker with the Gold Sequence

Starting with Hadamard-Walsh, we can see from Fig.6.7 that both sequences have similar positioning accuracy. However, the main issue with implementing this sequence is how to expand it to match the configuration needed. Moreover, in case we initialize it in a similar manner to Gold codes (by generating 4 bits from different Hadamard codes then initiate the QPSK symbols), the performance can't be predicted and it will show the same inconsistency as with original gold sequence when transmitting a single subframe.

In Fig.6.8, several ZC sequences of different lengths have been simulated, namely lengths of 63, 839 & 997. These values are chosen since 63 ZC sequence is used in PSS and 839 used for RACH procedure while 997 is chosen since it is the biggest prime number less than 1000. Based on the results, we can see clearly that ZC sequence of length 63 achieves a better accuracy compared to gold sequence for the simulated cell IDs, while for length 839 and 997, they are both comparable. Main implementation issues for using ZC sequences in positioning were introduced in Chapter 4 Section 4.4.1.

Looking into Fig.6.9, we can compare the performance of ZCC sequence with the original where ZCC shows a better accuracy. However, as mentioned in Section 4.4.3, due to the random part in ZCC generation, the constellation diagram can't resemble any conventional modulation schemes which make its implementation harder in reality.

In Fig.6.10, the Barker based code has been shown against original. In terms of performance, Barker shows a decent performance compared with the standard for the configured cell IDs. Despite the fact that Barker based code performed better, it still ambiguous how the performance of Barker with different cell IDs upon a proper expansion.

In terms of comparing different sequences, another property is worth considering which is Peak to Average Power Ratio (PAPR) to decide which sequence performs more efficiently. As can be seen in the next 2 figures 6.11 and 6.12, PAPR has been analyzed on both downlink (OFDM) and uplink (SC-FDMA) for the different sequences introduced before.

As shown in downlink, similar performance is observed while in Uplink, we can clearly note

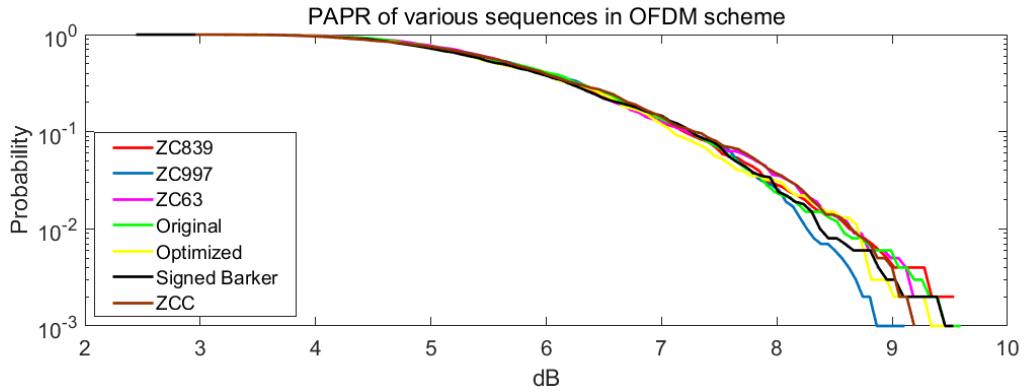


Figure 6.11: PAPR of various sequences in OFDM scheme

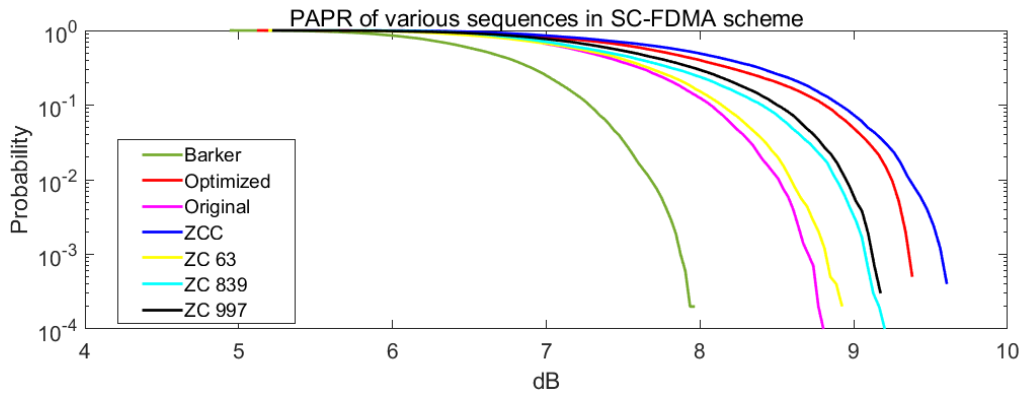


Figure 6.12: PAPR of various sequences in SC-FDMA scheme

that the complex constellation diagram such as ZCC and optimized sequences perform worse compared to standard QPSK modulation symbols configured with Gold and Barker sequences. In addition to sequences with constant envelope namely Zaddoff-Chu sequence slightly worse performance can be seen in comparison to Gold sequence.

As a summary, the characteristics and performances of different sequences are provided below:

6.5 Gold Sequence Optimization

The positioning accuracies of the optimized sequence are presented from Figs.6.13 to 6.16. The first three figures are based on the first optimization approach, introduced in Section 4.3 for different cell ID combinations. The last figure presents the second approach, with the Cell ID selected from 1 to 6. Regardless which optimization method used, the positioning accuracy is mostly better. Nevertheless, the drawback has been analyzed before, which is the huge requirements in calculation complexity and inflexibility in practice.

Table 6.2: Sequence Comparison

Criteria	Gold	ZC	H-W	ZCC	Barker
Complexity	low	low	low	High	low
Constellation Diagram	QPSK	M-PSK	BPSK/QPSK	complex	QPSK
Auto-Correlation Properties	Good	Good	Poor	Good	Good
Cross-Correlation Properties	Good	Good	Good	Good	Good
Accuracy	Standard	Comparable	Worse	Better	Better
PAPR Uplink	Similar Performance			Worse	Better
PAPR Downlink	Similar Performance				

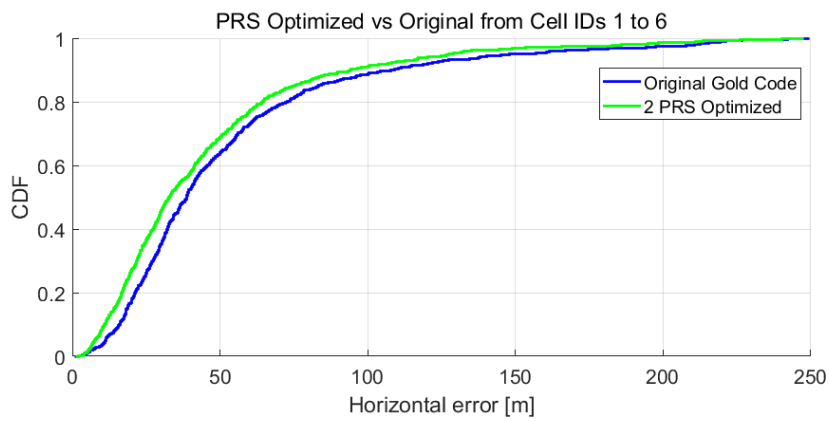


Figure 6.13: Optimized Sequence vs original for cell IDs from 1 to 6 1st approach

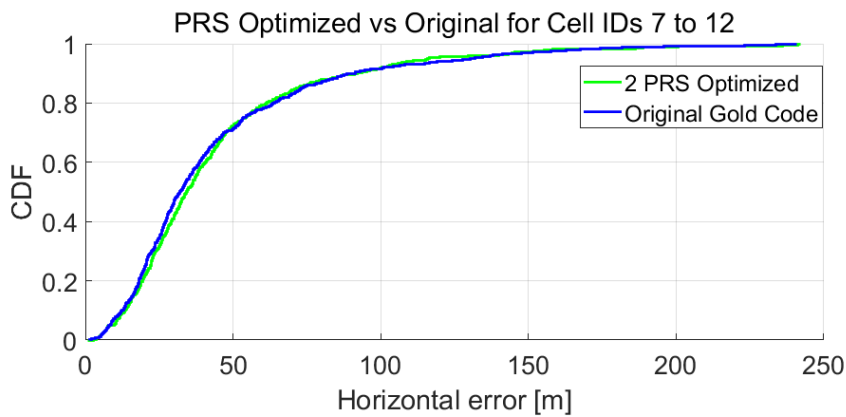


Figure 6.14: Optimized Sequence vs original for cell IDs from 7 to 12

6.6 Multiple Subframes processing

In order to further improve positioning accuracy multiple subframes carrying NPRS will be transmitted from transmitter and coherently combined at receiver side. Three modes of coherent

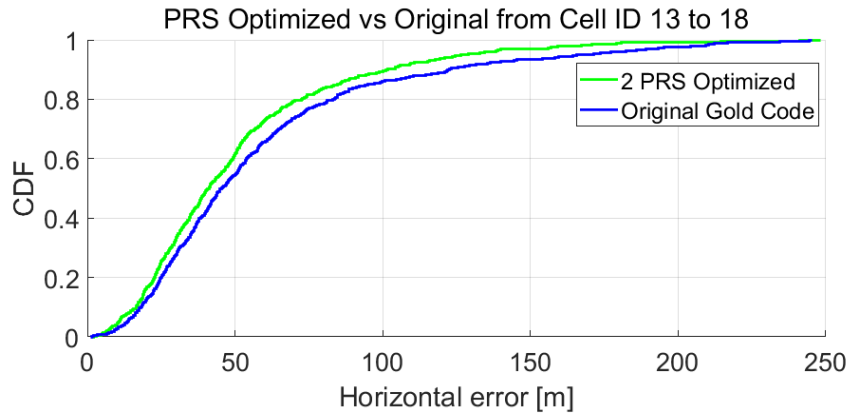


Figure 6.15: Optimized Sequence vs original for cell IDs from 13 to 18

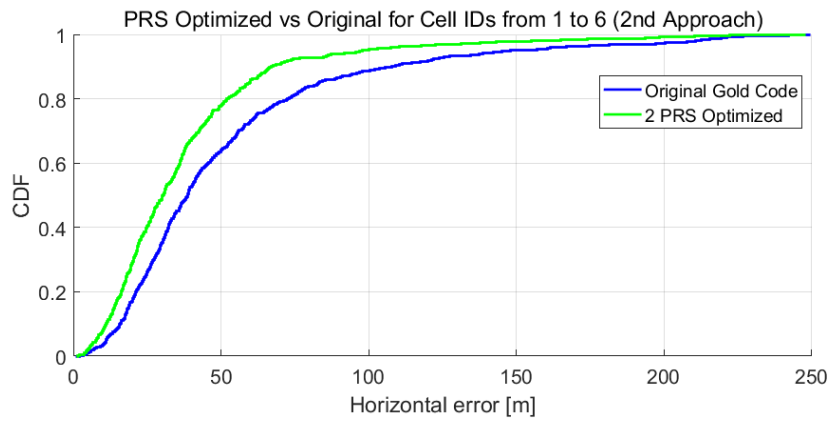


Figure 6.16: Optimized Sequence vs original for cell IDs from 1 to 6 2nd approach

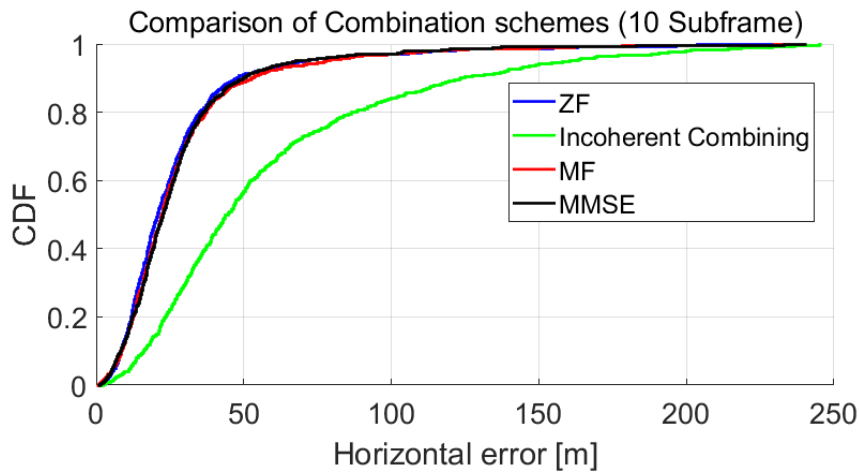


Figure 6.17: Coherent vs Incoherent Combining

combinations have been introduced in the thesis, MF, ZF and MMSE, as well as incoherent combination. In this section, initially, different combination types will be presented and compared

then the effect of sending more subframes will be analyzed with mostly Matched filter combination algorithm unless otherwise stated due to reduced computation time. It can be observed in Fig.6.17, coherent combining of different types performs better than incoherent combining due to the fact that channel effect has been reduced. In the next Figs.6.18 and 6.19, 30 subframes against 10 subframes and a single subframe of 2 different cell ID's configuration are shown. It is clearly noted that with 30 subframes, performance hugely improved by almost 30 meters in accuracy, while for 10 subframes, almost 20 meters in accuracy is gained over a single subframe for 70% of the UEs for cell IDs from 1 to 6. And almost same level of improvements can be denoted for cell IDs from 0 to 5.

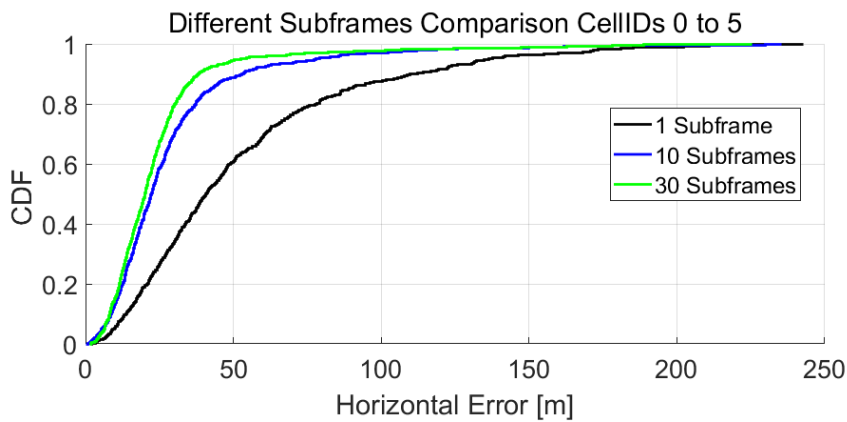


Figure 6.18: Multiple Subframes cell IDs from 0 to 5

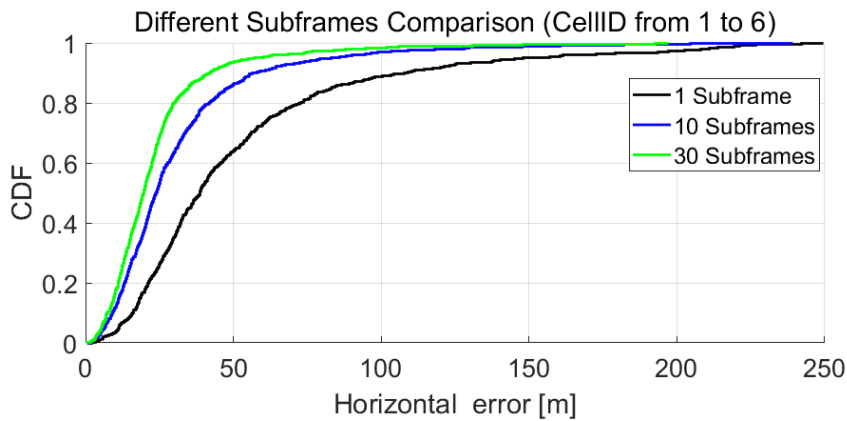


Figure 6.19: Multiple Subframes cell IDs from 1 to 6

6.7 Multiple PRBs processing

For applications beyond NB-IoT, more frequency subcarriers are reserved for NPRS transmission as introduced earlier in Section 4.5. In this section, we will analyze the accuracy improvements

when sending multiple PRBs in comparison to a single PRB as in Fig.6.20 then the effect of sending multiple PRBs with multiple subframes as in Figs.6.21 & 6.22. From Fig.6.20, we can see almost 47 meters of accuracy gained when occupying 4 PRBs and 34 meters when sending 2 PRBs when compared to a single PRB transmission for 70% of the UEs due to the fact that peak detection becomes easier.

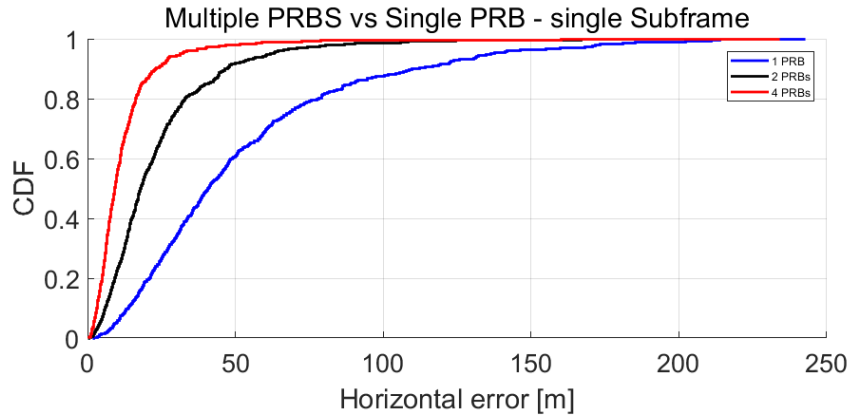


Figure 6.20: Multiple PRBs vs single PRB

In Figs.6.21 and 6.22, clear great accuracy improvements can be noted when sending multiple PRBs alongside multiple subframes which leads to clear understanding how much accuracy is better in higher bandwidths systems such as MTC and LTE in comparison to NB-IoT. In Fig.6.23, performance of different subframes and PRBs settings are shown together.

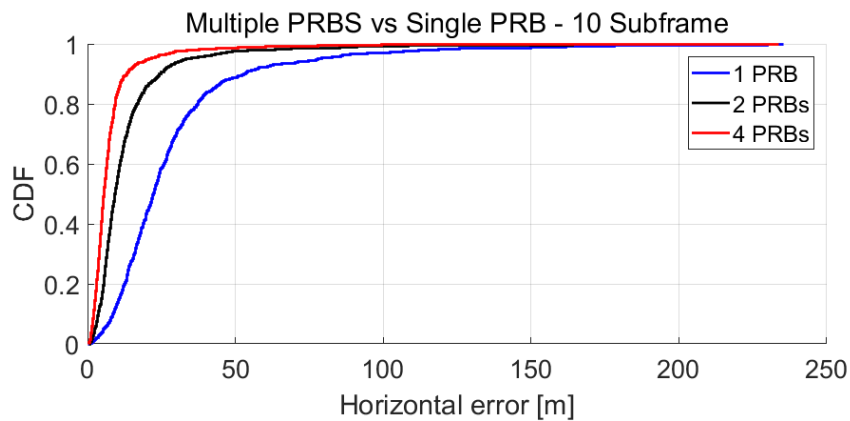


Figure 6.21: Multiple PRBs 10 subframes

6.8 EPA channel

In order to further evaluate the positioning accuracy performance, more realistic channel models with multi-path effect have been tested like EPA channel which introduced earlier in Chapter 5.

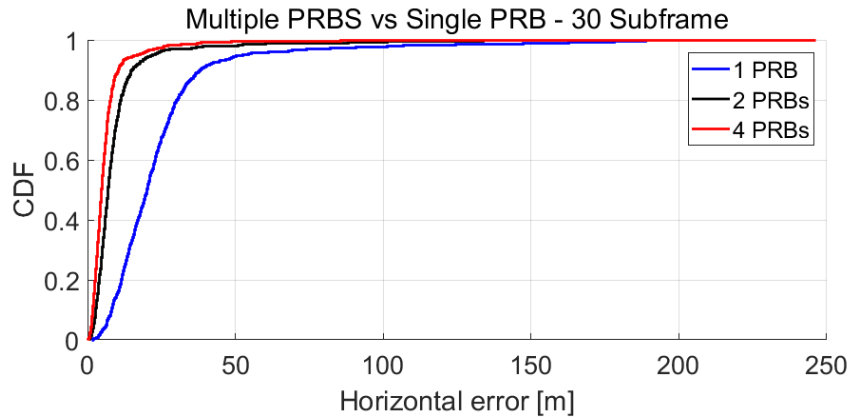


Figure 6.22: Multiple PRBs 30 subframes

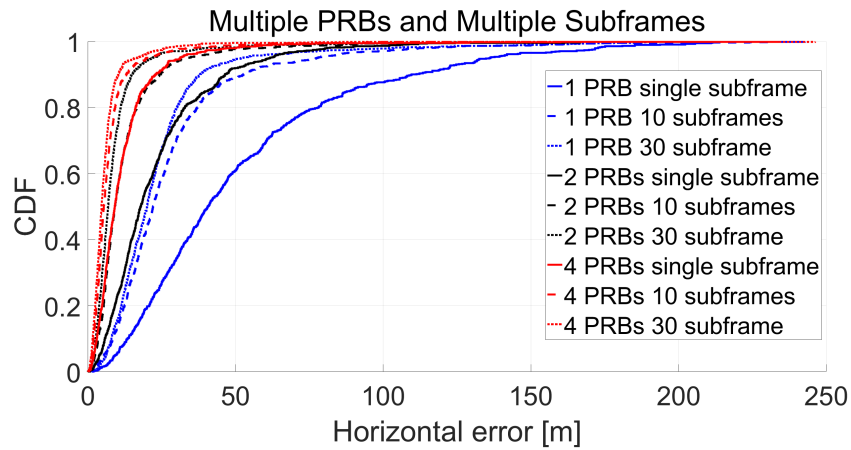


Figure 6.23: Multiple PRBs and subframes

As expected, positioning accuracy is far from satisfaction when sending a single subframe while improved when sending multiple subframes with coherent combining at receiver side, as shown in Fig.6.24, where over 60 meters accuracy is clearly gained.

Moreover, accuracy can be improved if more resources in frequency domain are utilized as illustrated in Fig.6.25 where 2 PRBs performance is compared to 1 PRB when sending 10 subframes at 10 dB SNR. As a conclusion, OTDOA positioning will perform better with LTE and MTC where more PRBs are configured.

In the incoming figure Fig.6.26, the optimized sequence using the first approach will be compared with the original where it shows slightly better accuracy. This figure shows performance for the cell IDs from 0 to 5, for other cell IDs, different accuracies are expected.

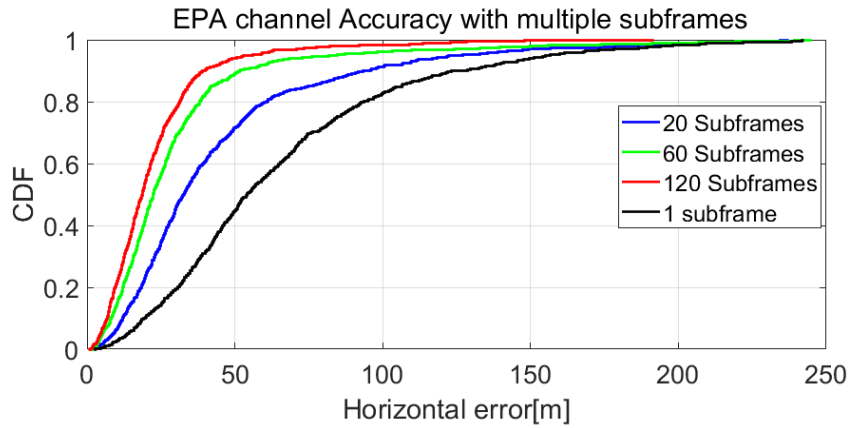


Figure 6.24: Multiple Subframes vs Single Subframe EPA Ch. 10dB SNR and 3Hz doppler

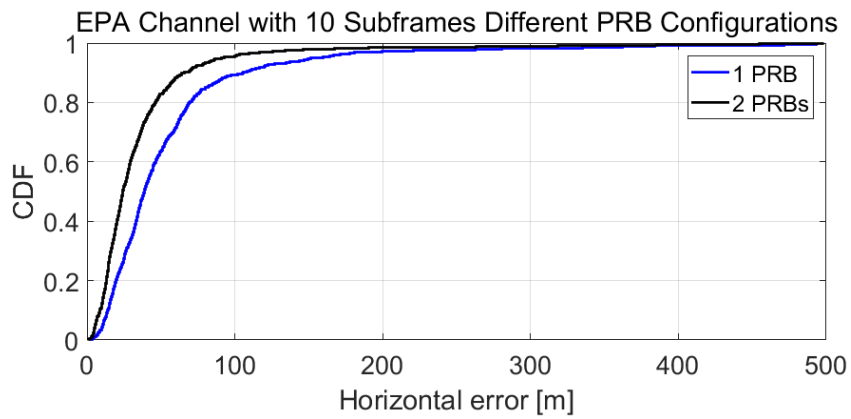


Figure 6.25: Different PRBs configuration Performance

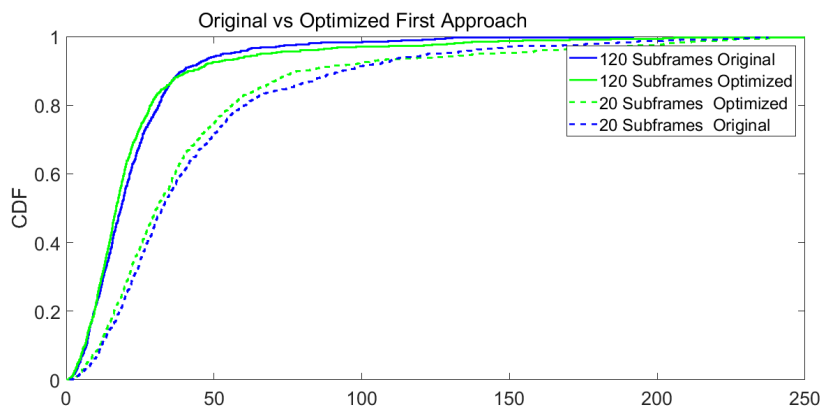


Figure 6.26: EPA channel Original and Optimized Positioning Accuracy

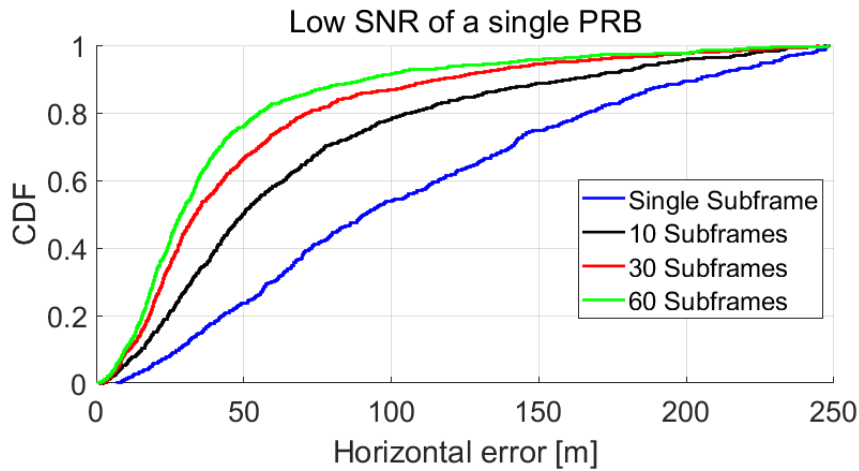


Figure 6.27: Low SNR with a single PRB

6.9 Low SNR Analysis

In order to further evaluate the performance of IoT OTDOA positioning accuracy, low SNR values need to be studied since most of NB-IoT devices, MTC or devices which will use OTDOA positioning algorithm will be in severe coverage conditions and operates with low SNR values such as -20dB or -10dB. So in the following figures, SNR value of -10 dB will be analyzed with AWGN channel. For more realistic results, it is of necessity to include channels with multi-path effect such as EPA and ETU as illustrated in the last two figures. As can be seen from the figures, positioning accuracy is much worse for UEs under -10dB in comparison to 10dB.

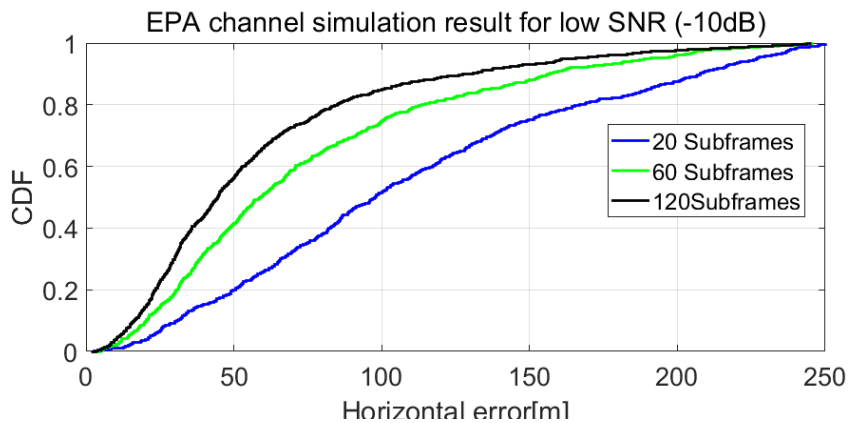


Figure 6.28: Low SNR EPA Channel

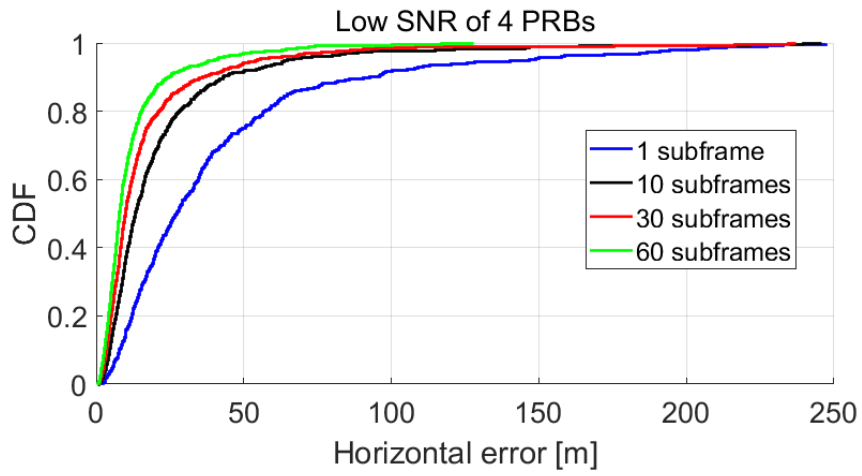


Figure 6.29: Low SNR with 4 PRBs

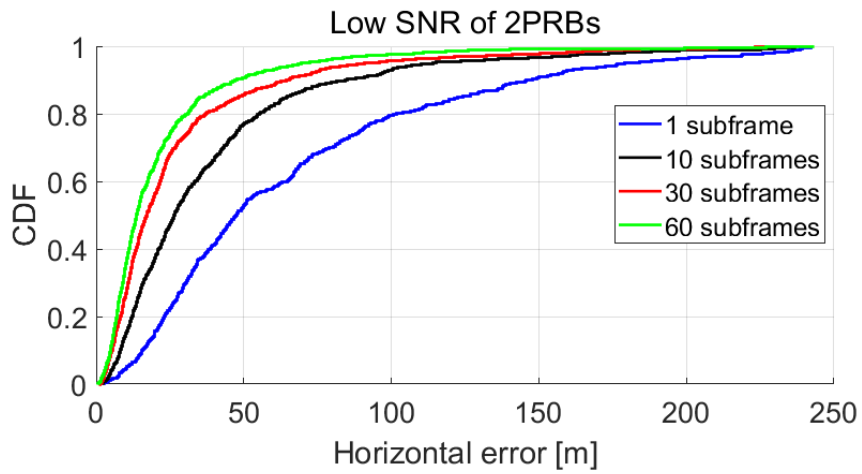


Figure 6.30: Low SNR with 2 PRBs

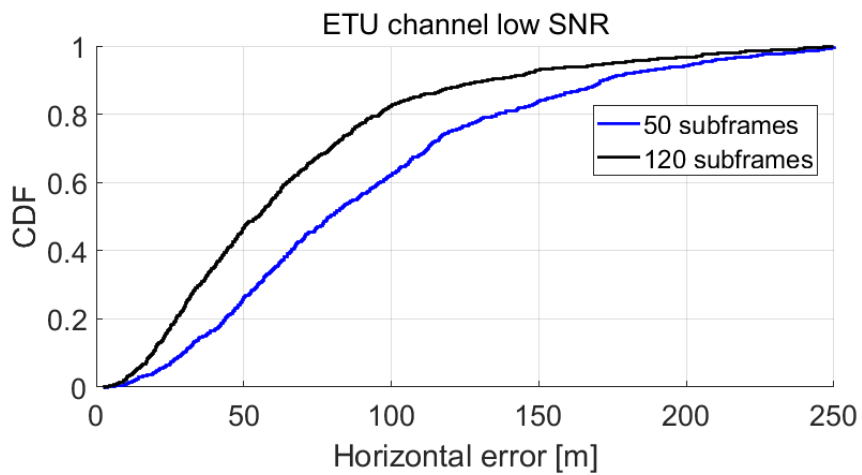


Figure 6.31: Low SNR ETU Channel with 3Hz doppler

SUMMARY

In this thesis project, several approaches related to PRS sequences and configuration have been implemented for the sake of enhancing IoT positioning accuracy. Those are listed and summarized as follows:

- First, increasing PRS density by sending more NPRS signals within an OFDM symbol may lead to a good autocorrelation shape. However, less eNBs can be accommodated following this design scheme and it leads to more inter cell interference once the number of eNBs increases.
- Secondly, the idea of redesigning the current resource grid may lead to an improvement for certain cell ID configurations. Nevertheless, all these new suggested redesigns show the same performance as legacy once tested with different cell ID combinations.
- An optimization approach of autocorrelation has been tested and it shows relatively satisfactory results but with the price of higher complexity and computation time, which constrains the possibility of utilizing this approach in reality for low power devices.
- Finally, different sequences instead of the current Gold sequence have been tested out. It is indicated that once the sequence mapped to QPSK symbols, regardless of which sequence used for implementation the positioning accuracy resembles that of the current legacy. However, there is still room for enhancement if more complex signal constellation is permitted at transmitter side and it is worth more investigation in the future.

In order to reduce the power consumption of NB-IoT devices, it is assumed that the receiver operates at low sampling-rate mode which in turn affects positioning accuracy results. Keeping

this in mind, it can be clearly seen how the positioning performance can be enhanced by up-sampling via interpolation with a decent SNR. More enhancement can be achieved by sending multiple subframes and combining them coherently at receiver side but with the trade-off of extra computational complexity. In terms of complexity and computation time MF performs the best. As to the correlator design, frequency domain correlator shows a similar positioning accuracy compared with the correlator operating in time domain, but with enhancement obtained in terms of computation speed.

Although current 3GPP standards are well designed, some improvement can still be obtained. In particular, the optimization method and certain sequences such as the Barker and ZC sequences give satisfactory positioning performances similar and in some occasions better than Gold sequence. Bear in mind that the accuracy differs for different cell IDs due to the fact that transmitted signal correlation properties changes. In terms of future work, further investigations on sequence designs that offer good performance accuracy, reasonable implementation complexity, and flexibility (i.e support many cell-IDs) can be conducted.

BIBLIOGRAPHY

- [1] Huawei, "Narrowband IoT wide range of opportunities," tech. rep., Nov. 2016.
- [2] S. Fischer, "OTDOA positioning in 3GPP LTE," tech. rep., 2014.
- [3] A. Berg, "OTDOA based positioning in NB-IoT," Master's thesis, 2017.
- [4] X. Lin, F. G. J. Bergman, O. Liberg, S. Razavi, H. Razaghi, H. Rydén, , and Y. Sui, "Positioning for the internet of things: A 3GPP perspective," Sep. 2017.
- [5] K.Rose, S.Eldridge, and L.Chapin, "The internet of things: An overview," *The Internet Society*, 2015.
- [6] Cisco, "The Zettabyte Era: Trends and analysis," 2016.
- [7] Ericsson, "Ericsson Mobility Report," tech. rep., Nov. 2016.
- [8] 3GPP, "Evolved Universal Terrestrial Radio Access (E-UTRA); Physical channels and modulation," Technical Specification (TS) 36.211, 3rd Generation Partnership Project (3GPP), 2017, Version 14.4.0.
- [9] O.Liberg, M.Sundberg, Y.-P. E. Wang, J. Bergman, and J. Sachs, *Cellular Internet of Things: Technologies, Standards, and Performance*. Mara E. Conner, 2018.
- [10] A. Adhikary, X. Lin, and Y.-P. E. Wang, "Performance evaluation of NB-IoT coverage," 2016.
- [11] Ericsson, "Cellular networks for massive IoT," Ericsson, Jan. 2016.
- [12] R. Prasad, *OFDM for Wireless Communication Systems*. Artech House, 2004.
- [13] Spirent, "An overview of LTE positioning," Feb. 2012.
- [14] J. Figueiras and S. Frattasi, *Mobile Positioning and Tracking: from conventional to cooperative techniques*. Wiley, 2010.

BIBLIOGRAPHY

- [15] 3GPP, “Evolved Universal Terrestrial Radio Access (E-UTRA); LTE Positioning Protocol,” Technical Specification (TS) 36.355, 3rd Generation Partnership Project (3GPP), 2017, Version 14.3.0.
- [16] R. . Schwarz, “LTE location based services,” 2012.
- [17] 3GPP, “Evolved Universal Terrestrial Radio Access (E-UTRA); Physical layer; Measurements,” Technical Specification (TS) 36.214, 3rd Generation Partnership Project (3GPP), 2017, Version 14.3.0.
- [18] 3GPP, “Evolved Universal Terrestrial Radio Access (E-UTRA); Requirements for support of radio resource management,” Technical Specification (TS) 36.133, 3rd Generation Partnership Project (3GPP), 2017, Version 14.4.0.
- [19] S.Sesia, I.Toufik, and M.Baker, *LTE The UMTS Long Term Evolution from Theory to Practice*. Wiley, 2011.
- [20] R. Frank, S. Zado, and R. Heimiller, “Phase shift pulse codes with good periodic correlation properties,” *IRE Transactions on Information Theory*, vol. 8, pp. 381–382, 1962.
- [21] D. Chu, “Polyphase codes with good periodic correlation properties ,” *IEEE Transactions on Information Theory*, vol. 18, pp. 531–532, 1972.
- [22] M. Viswanathan, *Simulation of Digital Communication Systems using MATLAB 2nd edition*. Mathuranathan Viswanathan at Gaussianwaves, 2013.
- [23] K. GERLACH and J. F. F. KRETSCHMER, “General forms and properties of zero cross-correlation radar waveforms,” tech. rep., Washington, DC 20375-5000, Jan. 1990.
- [24] J. F.F. Kretschmer and K. Gerlach, “Radar waveforms derived from orthogonal matrices,” tech. rep., Washington, DC 20375-5000, Feb. 1989.
- [25] K. MacDonald, “Barker sequences theory and applications,” Master’s thesis, 2009.
- [26] 3GPP, “Evolved Universal Terrestrial Radio Access (E-UTRA); Base Station (BS) radio transmission and reception,” Technical Specification (TS) 36.104, 3rd Generation Partnership Project (3GPP), 2017, Version 14.3.0.
- [27] A. F. Molisch, *Wireless Communications: Principles and Practice*. Wiley, 2011.
- [28] A. Paulraj, R. Nabar, and D. Gore, *Introduction to Space-Time Wireless Communications*. Cambridge Universtiy Press, 2003.
- [29] A. V. Oppenheim, R. W. Schaffer, and J. R. Buck, *Discrete Time Signal Processing*. Prentice Hall, 1999.

- [30] R. G. Lyons, *Understanding Digital Signal Processing*.
Prentice Hall, 2011.
- [31] S. M. Kay, *Fundamentals of Statistical Signal Processing, Volume I: Estimation Theory*.
Prentice Hall, 2011.
- [32] 3GPP, “R1-168310 WF on simulation assumption for NB-IoT positioning,” tech. rep., 3rd
Generation Partnership Project (3GPP), 2016.



LUND
UNIVERSITY

Series of Master's theses
Department of Electrical and Information Technology
LU/LTH-EIT 2018-647
<http://www.eit.lth.se>